

RESEARCH

Open Access



# Development of autonomic innervation at the venous pole of the heart: bridging the gap from mice to human

Fleur Zwanenburg<sup>1,6</sup> , Thomas A. Bos<sup>2</sup>, Arend D. J. Ten Harkel<sup>3,6</sup>, Monique C. Haak<sup>1,6</sup>, Nathan D. Hahurij<sup>3,6</sup>, Robert E. Poelmann<sup>2,4</sup>, Conny J. van Munsteren<sup>2</sup>, Lambertus J. Wisse<sup>2</sup>, Nico A. Blom<sup>3,6</sup>, Marco C. DeRuiter<sup>2,6</sup> and Monique R. M. Jongbloed<sup>2,5,6\*</sup> 

## Abstract

**Background** Prenatal development of autonomic innervation of sinus venosus-related structures might be related to atrial arrhythmias later in life. Most of the pioneering studies providing embryological background are conducted in animal models. To date, a detailed comparison with the human cardiac autonomic nervous system (cANS) is lacking. The aim of this study was to compare the morphological and functional development of the cANS between mouse and human, specifically aimed at the venous pole.

**Methods** Wildtype mouse embryos (E9.5–E18.5) and healthy human fetuses (6–38 weeks gestational age (WGA)) were studied at sequential stages to obtain a comparative developmental series. Cardiac autonomic function was assessed through heart rate variability (HRV) analysis using ultrasound. Morphological assessment of the venous pole was performed using immunohistochemical stainings for neural crest cells and autonomic nerve markers.

**Results** Murine cANS function did not definitively establish in utero as HRV parameters depicted no trend prior to birth. In contrast, human HRV parameters greatly increased from 20 to 30 WGA, indicating that human cANS function is established prenatally around 20 WGA and matures thereafter. Morphologically, cANS development followed a similar sequence with neural crest-derived nerves entering the venous pole in proximity to the developing pulmonary vein in both species. However, the timing of differentiation into sympathetic or parasympathetic phenotype was markedly distinct, as human autonomic markers emerged relatively later when related to major cardiogenesis. Structures related to arrhythmogenicity in humans, such as the ligament/vein of Marshall and the myocardium surrounding the pulmonary veins, become highly innervated during embryonic development in both mice and humans.

**Conclusion** Although early morphological cANS development at sinus venosus-related structures follows a similar sequence in mice and humans, there are substantial differences in the timing of functional establishment and differentiation in sympathetic and parasympathetic phenotypes, which should be taken into account when extrapolating mouse studies of the cANS to humans. The abundant innervation of sinus venosus-related structures may play a modulatory role in arrhythmogenesis under pathological conditions.

**Keywords** Arrhythmia, Cardiac autonomic nervous system, Cardiac innervation, Neural crest, Venous pole, Pulmonary veins, Prenatal development, Heart rate variability

\*Correspondence:

Monique R. M. Jongbloed  
[m.r.jongbloed@lumc.nl](mailto:m.r.jongbloed@lumc.nl)

Full list of author information is available at the end of the article



© The Author(s) 2025. **Open Access** This article is licensed under a Creative Commons Attribution-NonCommercial-NoDerivatives 4.0 International License, which permits any non-commercial use, sharing, distribution and reproduction in any medium or format, as long as you give appropriate credit to the original author(s) and the source, provide a link to the Creative Commons licence, and indicate if you modified the licensed material. You do not have permission under this licence to share adapted material derived from this article or parts of it. The images or other third party material in this article are included in the article's Creative Commons licence, unless indicated otherwise in a credit line to the material. If material is not included in the article's Creative Commons licence and your intended use is not permitted by statutory regulation or exceeds the permitted use, you will need to obtain permission directly from the copyright holder. To view a copy of this licence, visit <http://creativecommons.org/licenses/by-nc-nd/4.0/>.

## Introduction

The cardiac autonomic nervous system (cANS) plays a pivotal role in maintaining cardiovascular homeostasis by adapting cardiac function in response to external demands. Although the mechanism of cardiac autonomic modulation is highly complex, generally, sympathetic (adrenergic) activation arising from the paravertebral sympathetic chains elicits an increase in heart rate, contraction force and conduction velocity, while parasympathetic (cholinergic) stimulation originating from the vagal nerve has the opposite effect [1, 2]. This adaptability of the cANS is well reflected in the alterations of the heart rate, also known as heart rate variability (HRV). In the healthy and mature state, the two branches of the cANS act in equilibrium resulting in a considerable HRV, which is mandatory from fetal to adult life to respond to physiological and pathophysiological stimuli. However, during aging and pathological conditions, extensive remodeling of the cANS can lead to regional and temporal dominance of the sympathetic nervous system, both functionally and morphologically. This is associated with adverse outcomes during prenatal and postnatal life, such as uteroplacental dysfunction, intrauterine fetal demise, sudden infant death, and cardiac events or sudden death in adults with or without known cardiovascular disease [3–9].

Over the last decades, autonomic imbalance has garnered particular interest in the field of cardiac arrhythmias as sympathetic predominance is linked to the genesis and maintenance of atrial arrhythmias [10–12].

A significant proportion of atrial arrhythmias find their origin at specific predilection sites which are primarily derived from the myocardium at the venous pole of the heart, such as the terminal crest, the ostium of the coronary sinus, the ligament of Marshall, and the myocardial sleeves of the pulmonary and caval veins [13–15]. It has previously been observed that the development of the embryonic cardiac conduction system relates to these areas, suggesting that this may contribute to atrial arrhythmias later in life, possibly by the re-expression of a fetal program [16–19]. As the cANS is an important modulator of the cardiac conduction system, understanding cANS development in relation to the venous pole seems fundamental to further unravel the complexities of arrhythmogenesis.

Embryonic cANS development is a complex process that involves numerous cell types, genes, and their interactions [1, 12]. Depending on their axial level of origin, neural crest cells (NCCs) generate cardiac sympathetic and parasympathetic neurons after migrating from the region overlaying the dorsal neural tube (Fig. 1) [20–23]. Cardiac nerves enter the heart through both the arterial and venous poles. Nerves entering via the arterial pole primarily innervate the ventricles, aorta and coronary arteries, while those entering through the venous pole supply nerves to both the atria and ventricles [24]. Notably, mammalian NCC migration and differentiation into cardiac autonomic (i.e. sympathetic or parasympathetic) neurons has predominantly been studied in mice [12,

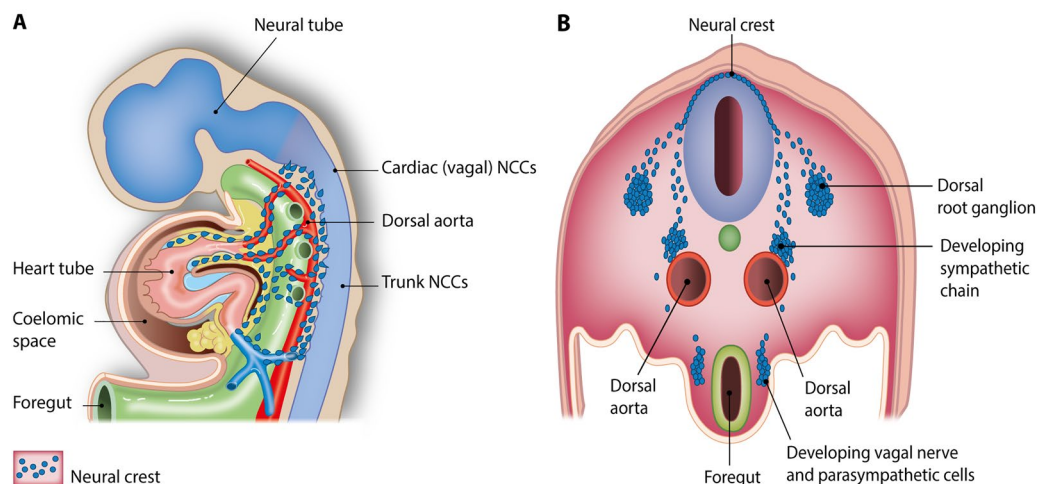


**Fig. 1** Embryology of cardiac autonomic innervation. **A** Cardiac autonomic nerves at the arterial and venous poles are primarily derived from neural crest cells (NCCs; dark blue dots), multipotent cells migrating from the neural tube region. Parasympathetic nerves emanate from the cranially situated cardiac (vagal) NCCs while sympathetic nerves originate from trunk NCCs. **B** Cardiac (vagal) NCCs, precursors of parasympathetic nerve cells, migrate along the developing vagal nerve pathway directly towards the heart to form the cardiac parasympathetic ganglia. From there, parasympathetic nerve projections extend to the venous pole. Trunk NCCs, precursors of sympathetic nerve cells, migrate ventrally towards the dorsal aortae to form the paravertebral sympathetic trunks. From there, sympathetic nerves extend into the heart through the cardiac plexus alongside the previously developed vagal nerves. **B** is modified after Vegh et al. [1], published open access under Creative Commons Attribution License (CC BY)

22]. However, the development of the venous pole differs markedly between humans and mice: the left superior caval vein persists in mice, whereas in humans this structure regresses to form the ligament of Marshall, that contains numerous epicardial ganglionated nerves supplying the dorsal surface of the ventricles and left atrium [25]. Moreover, adult mice generally exhibit a predominant sympathetic tone while adult humans tend to have a predominant parasympathetic tone [26]. Together, this raises the question of whether the murine embryo is a suitable model for studying human cANS development, both from a morphological and functional perspective. To our knowledge, no comparative studies between mice and humans during the prenatal period exist. This study aims to bridge this gap by providing a comparative analysis of murine and human prenatal cANS development at the venous pole at sequential prenatal stages, both functionally and morphologically.

## Material and methods

A schematic representation of the experimental setup is depicted in Supplemental Fig. 1.

### Heart rate variability recordings in mouse embryos

To study functional cANS development in mouse embryos, heart rate variability (HRV) analysis was assessed in vivo on heart rate recordings obtained by high frequency ultrasound. HRV analysis is a tool that quantifies the variation between two consecutive heartbeats, where each derived HRV parameter reflects a different aspect of cANS activation or maturation. Heart rate recordings were conducted on wildtype mouse embryos (C57BL/6J background) ranging between E9.5 and E18.5 ( $n=49$ ) using the Vevo3100 ultrasound system (FUJIFILM VisualSonics, Toronto, Canada), with a 40 MHz transducer. Ultrasound examinations were performed longitudinally at 2 subsequent stages between E9.5 and E18.5 (either E9.5 and E13.5, E11.5 and E15.5, or E13.5 and E18.5), or solely at E9.5 to include tissue for histological examination at this early stage. Identification of the individual mouse embryos at the second examination was based on their position in the maternal abdomen, with the maternal bladder used as reference point. All ultrasound examinations were performed by FZ and CJM under similar conditions using a previously described experimental setup [27]. Pregnant mother mice ( $n=14$ ) were sedated with isoflurane anesthesia via a cone-shaped nose mask (induction 4% isoflurane; maintenance 1.5% isoflurane). During the study recordings, isoflurane delivery was continuously adjusted to maintain maternal vital signs at a cardiac frequency of 400–600 beats per minute, respiratory rate of 45–75 breaths per minute and body temperature 36.5–37.5°C. Heart rate

recordings were performed after at least 5 min of maintenance anesthesia and consisted of pulsed-wave Doppler recordings over the (future) cardiac valves of all individual embryos. We aimed to record in- and outflow simultaneously by placing the Doppler sample volume across both the (future) common atrioventricular orifice and (future) common outflow tract orifice at the early stages E9.5 and E11.5, and across the (future) mitral valve and (future) aortic valve at stages E13.5, E15.5 and E18.5. If a simultaneous recording was not feasible, in- and outflow were assessed separately. Each recording comprised 10 s and was repeated until 3 high-quality recordings were secured. Scanning time was kept as short as possible to limit a possible effect of isoflurane anesthesia on the measurements. Although the examiners were not blinded to gestational age, beat-to-beat intervals and the automatically derived HRV values were not visible during recordings. Beat-to-beat intervals for HRV analysis were obtained through offline analysis using VisualSonics analytical software (Vevo LAB version 5.6.1, FUJIFILM VisualSonics, Toronto, Canada) (Supplemental Fig. 1A). HRV parameters were calculated separately from 3 high-quality beat-to-beat recordings and their mean value was used for final analysis. Embryos that displayed ectopic heartbeats were excluded from HRV analysis, as HRV analysis requires sinus rhythm in order to study the true vagosympathetic input into the sinoatrial node (SAN). The following short-domain HRV parameters were assessed according to the HRV Task Force guidelines [28]: SDNN, RMSSD, SDNN/RMSSD ratio, pNN10 (Table 1). Due to the short recording times (fetal movements impede longer recordings), SDNN mainly represents short-term vagal activity.

### Heart rate variability recordings in human fetuses

To assess functional cANS development in human embryos, in vivo heart rate recordings of human fetuses ( $n=18$ ) were conducted longitudinally throughout gestation using color Tissue Doppler Imaging (cTDI), an advanced and accurate ultrasonographic technique [29]. The comprehensive methods and results of these functional measurements have been published previously [30]. For the current study, we processed these data as reference against the morphological human data and data derived from mice. In brief, healthy pregnant mothers with singleton pregnancies ( $n=18$ ) were subjected to 3 or 4 ultrasound examinations between 13 and 38 weeks gestational age (WGA), with an inter-examination interval of 8 weeks. Each participant was included at various gestational ages ( $n=2-3$  per week of gestation) to study the full prenatal time course. Of note, accurate heart rate recordings before 13 WGA are not feasible, as our previous study demonstrated technical limitations in cTDI

**Table 1** HRV parameters studied in murine and human embryos

HRV parameter	Description	Interpretation
SDNN	Standard deviation of all normal-to-normal interbeat intervals (ms)	Total variability (in clips of 10 s, mainly representing vagal activity)
RMSSD	Root mean square of successive differences between normal-to-normal beats (ms)	Parasympathetic control
SDNN/RMSSD ratio	Ratio between SDNN and RMSSD	Sympathovagal balance
pNN10	Proportion of normal-to-normal beat intervals differing more than 10 ms (%)	Very short time variation regulated by parasympathetic activity

recordings between 10 and 13 WGA [30], and Doppler recordings before 10 WGA are discouraged for safety concerns. All ultrasound examinations were performed by FZ under similar conditions using the Canon Aplio i-800 ultrasound machine with abdominal PVI475BX and PVT674 High Frequency convex transducers (Canon Medical Systems Europe B.V., Zoetermeer, Netherlands). Study recordings consisted of cTDI cine loops of the apical or basal cardiac four-chamber view. Each recording comprised 10 s and was repeated 10 times. Although the examiner was not blinded to gestational age, beat-to-beat intervals and the automatically derived HRV values were not visible during recordings. The ultrasound recordings were analyzed offline using a measurement software package provided by Canon Medical Systems that automatically labeled the beat-to-beat intervals from the myocardial velocity curve generated by cTDI (region of interest placed around the entire cardiac four-chamber view) (Supplemental Fig. 1B). For each examination, HRV analysis was performed on 3 clips with the best recording quality of the myocardial velocity curve, their mean value was used for final statistical analysis. Similar to the embryonic mice, the following short-domain HRV parameters were assessed: SDNN, RMSSD, SDNN/RMSSD ratio, pNN10 (Table 1).

#### Immunohistochemistry of embryonic mouse heart specimens

To associate functional measurements with the morphological development of cardiac autonomic innervation, mother mice were sacrificed by cervical dislocation following the last ultrasound examination (at either E9.5, E11.5, E13.5, E15.5 or E18.5) and embryos were harvested for histological examination. For a better understanding of early development, the series was complemented with stages E10.5 and E12.5 of wildtype C57BL/6J mouse embryos from the Leiden Collection Cardiac Microscopy Series, which holds an extensive collection of stained and unstained slides from diverse cardiac specimens of various species and ages. All cardiac specimens were treated

similarly according to routine immunohistochemistry protocols: either the whole embryo or solely the thorax (depending on the developmental stage) was fixed in 4% paraformaldehyde phosphate (PFA) buffer pH 7.4 for 24–48 h, embedded in paraffin and transversely sectioned at 5  $\mu$ m thickness. Immunohistochemistry was performed as described previously (n=3 per developmental stage) [31, 32], using primary antibodies against autonomic nerve markers (general nerve marker tubulin beta 3 class III (TUBB3) (Santa Cruz Biotechnology, Inc. SC-80005, 1/1000), sympathetic nerve marker tyrosine hydroxylase (TH) (Thermo Scientific PA1-4679, 1/1000), parasympathetic nerve marker choline O-acetyltransferase (ChAT) (Abcam ab181023, 1/1000)), and primary antibodies that distinguish the SAN and sinus venosus myocardium from atrial myocardium (hyperpolarization activated cyclic nucleotide gated potassium channel 4 (HCN4), a cardiac conduction system marker (Alomone labs APC-052, 1/1000); tropomyosin, a myocardial marker (Sigma T9283, 1/1000) and Nkx2.5, a mesenchymal/myocardial second heart field marker (Santa Cruz Biotechnology SC-8697, 1/4000). In addition, Wnt1Cre;mT/mG reporter mouse embryos [32] were stained for enhanced green fluorescent protein (eGFP) (Abcam ab13970 1/500) to study neural crest cell contributions through lineage tracing. Primary antibodies were visualized with respective Alexa-conjugated fluorescent secondary antibodies (1/200, all purchased from Invitrogen). Finally, slides were counterstained with DAPI (1/1000, Life Technologies) to visualize cell nuclei and subsequently mounted with ProLong Gold (Life Technologies). High-resolution microscopy images were taken with the digital slide scanners 3DHitech Panoramic 250 Flash III and Zeiss Axio Scan.Z1.

#### Immunohistochemistry of human fetal heart specimens

Morphological development was assessed on human embryos/fetuses without signs of developmental defects ranging between 6 and 20 WGA (4–18 weeks postfertilization) (n = 11), obtained from the historical collection

of human embryos/fetuses at the department of Anatomy & Embryology of the Leiden University Medical Center (included in the local biobank “Congenital heart disease”), and from the local biobank “Ectopic pregnancy” which holds early fetal tissues after surgical removal of an ectopic pregnancy. Either the whole embryo or solely cardiac specimens were fixed in 4% PFA buffer, embedded in paraffin and transversely sectioned. Unstained sections from the historical collection (n=6) were stained for autonomic nerve markers TUBB3 (Santa Cruz Biotechnology, Inc. SC-80005, 1/1000), TH (Thermo Scientific PA1-4679, 1/1000) and ChAT (Abcam ab181023, 1/500) and myocardial marker tropomyosin (Sigma T9283, 1/1000) as described above. After counterstaining with DAPI (Life Technologies, 1/1000), slides were shortly incubated with TrueBlack (Biotum PI-230007, 1/20 dissolved in 70% ethanol) to quench autofluorescence. To study NCC contribution, 4 hearts of the historical collection that were stained for HNK-1 (expressed in migrating NCCs [33]; Hybridomabank, 1/50) and anti-muscle actin antibody HHF-35 staining (myocyte marker; Dako M635, 1/500) as described [34] were reevaluated. To distinguish NCCs from the cardiac conduction system cells, selected sections were stained with HCN4 Alomone labs APC-052, 1/1000). In addition, more recently collected embryonic heart tissue (n=1) obtained from an ectopic pregnancy was stained for TUBB3, TH, ChAT, tropomyosin, HCN4 and HNK-1 as described above. Of note, although HNK-1 has been successfully used to label early migrating NCCs in humans by our group and others [33, 35], it has also been reported to label cells not derived from NCCs, such as the developing cardiac conduction system [34]. However, as an exclusive marker to NCCs is currently lacking in humans [36], we consider HNK-1 as useful antigen. Careful interpretation in combination with a broad set of markers including neuronal and conduction system markers was performed for the current study to ensure proper interpretation of labelling, as previously recommended [36]. High-resolution microscopy images were taken with the digital slide scanners

3DHistech Panoramic 250 Flash III and Zeiss Axio Scan.Z1.

### Definitions

All morphological data was compared between mice and humans per major stage of cardiogenesis. Early cardiogenesis was defined as the looping phase of the myocardial heart tube (mouse E9.5–11.5 vs human 6–7 WGA). Mid-cardiogenesis was defined as the phase of four-chamber modeling (mouse E12.5–E14.5 vs human 7–9 WGA). Late cardiogenesis was defined as the phase in which the heart has adopted its definitive anatomical configuration (mouse  $\geq$  E15.5 vs human  $\geq$  10 WGA). Moreover, our interpretation of applied markers in mice and humans is detailed in Table 2.

### Statistics

All statistics were performed with SPSS Statistics 25.0 (IBM Corp., Armonk, New York, USA) and R Statistical software version 4.2.2 (Foundation for Statistical Computing, Vienna, Austria). Normally distributed variables were described using mean  $\pm$  standard deviation (SD), and continuous variables with skewed distributions were described using interquartile ranges (IQR). Trends over time for HRV parameters in both mice and human embryos/fetuses were analyzed using linear mixed-effects models, including a random intercept and slope per subject and as covariates the age at examination, mean embryonic/fetal heart rate and sex. This model accounts for the correlation between repeated measurements within subjects and allows different timings of examinations and missing values. To determine true time trends, cubic splines were used with knots at percentiles of the data and the number of knots chosen based on model fit (Akaike information criterion (AIC)). For all HRV parameters in mouse embryos, no knots (a linear trend) was identified as best model. In human fetuses, a linear trend was identified as best model to depict average HR and pNN10, whereas spline function with 2 or 3 knots fitted best with SDNN, RMSSD and SDNN/

**Table 2** Definition and interpretation of applied markers

Tissue type	Set of markers in mice	Set of markers in humans
Sinus venosus myocardium	HCN4 <sup>+</sup> /NKx2.5 <sup>-</sup> /tropomyosin <sup>+</sup>	HCN4 <sup>+</sup> /NKx2.5 <sup>-</sup> /tropomyosin <sup>+</sup>
Atrial myocardium	HCN4 <sup>-</sup> /NKx2.5 <sup>+</sup> /tropomyosin <sup>+</sup>	HCN4 <sup>-</sup> /NKx2.5 <sup>+</sup> /tropomyosin <sup>+</sup>
Neural crest(-derived) cells	eGFP <sup>+</sup>	HNK-1 <sup>+</sup> /HCN4 <sup>-</sup>
Undifferentiated nervous tissue	TUBB3 <sup>+</sup> /TH <sup>-</sup> /ChAT <sup>-</sup>	TUBB3 <sup>+</sup> /TH <sup>-</sup> /ChAT <sup>-</sup>
Sympathetic nervous tissue	TUBB3 <sup>+</sup> /TH <sup>+</sup> /ChAT <sup>-</sup>	TUBB3 <sup>+</sup> /TH <sup>+</sup> /ChAT <sup>-</sup>
Parasympathetic nervous tissue	TUBB3 <sup>+</sup> /TH <sup>-</sup> /ChAT <sup>+</sup>	TUBB3 <sup>+</sup> /TH <sup>-</sup> /ChAT <sup>+</sup>
Intrinsic cardiac adrenergic cells	TUBB3 <sup>-</sup> /TH <sup>+</sup> /ChAT <sup>-</sup>	TUBB3 <sup>-</sup> /TH <sup>+</sup> /ChAT <sup>-</sup>

RMSSD. Sampling error was quantified using 95% confidence intervals (CI).

## Results

### Functional development of cardiac autonomic activity in mice and humans

#### *High frequency prenatal ultrasound in mouse embryos shows frequent ectopic beats and tachycardia*

A total of 49 mouse embryos were assessed by high frequency ultrasound, which resulted in 72 individual recordings (E9.5 n=22, E11.5 n=8, E13.5 n=19, E15.5 n=7, E18.5 n=16). Median scanning time per embryo was 8 min (IQR 5–16 min). Remarkably, frequent ectopic

heartbeats were observed during 22 study recordings (30.6%) and were therefore excluded from HRV analysis (Fig. 2). Ectopic beats occurred in the majority of embryos at E13.5 (16/19, 84.2%), and to a lesser extent at E11.5 (3/8, 37.5%) and E18.5 (3/16, 18.8%). They were not encountered at stages E9.5 and E15.5. No difference was found in potential confounding factors between those with and without ectopic activity, as we found similar duration of scanning time (and thus duration of anesthesia) at onset of the ectopic beats (31.0 (IQR 21.0–41.75) vs 30.0 (IQR 17.0–41.0) minutes respectively,  $p=0.759$ ) and similar maternal vital signs during the ultrasound examination, indicating similar anesthesia depth

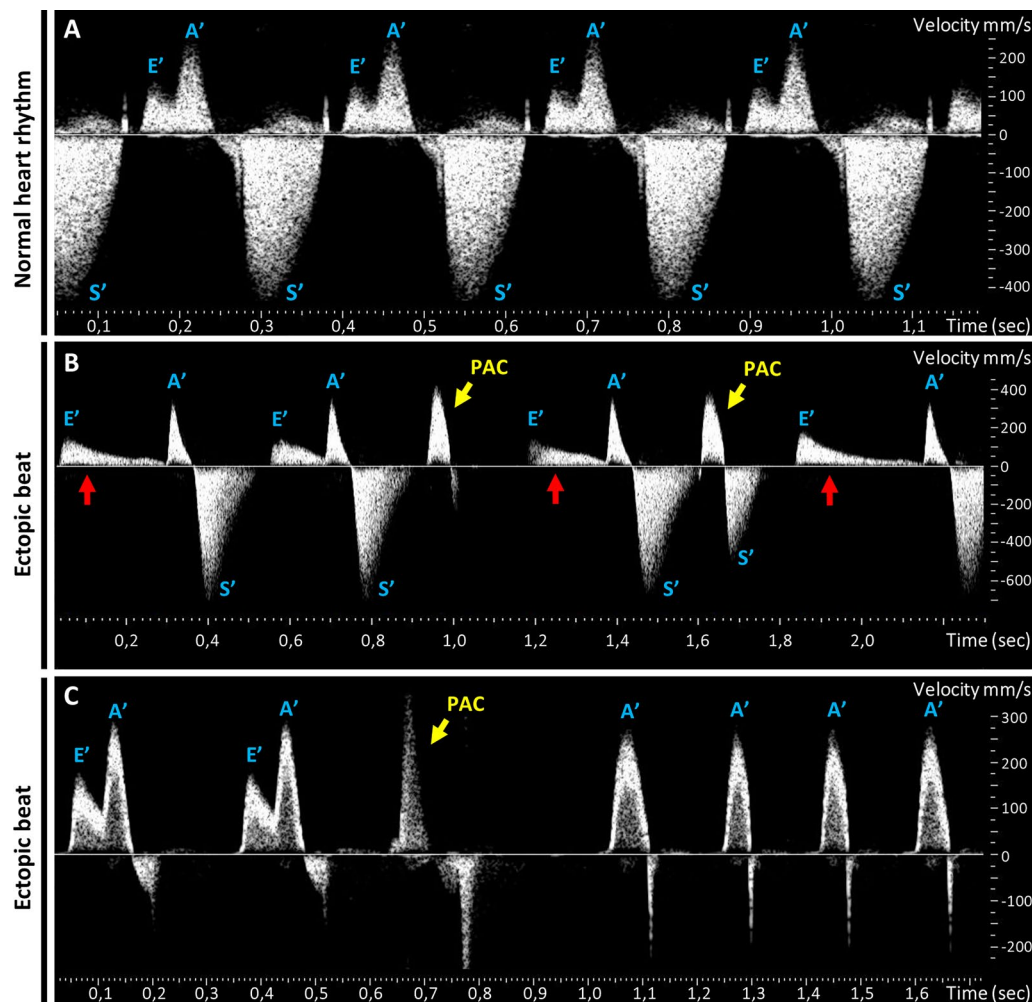
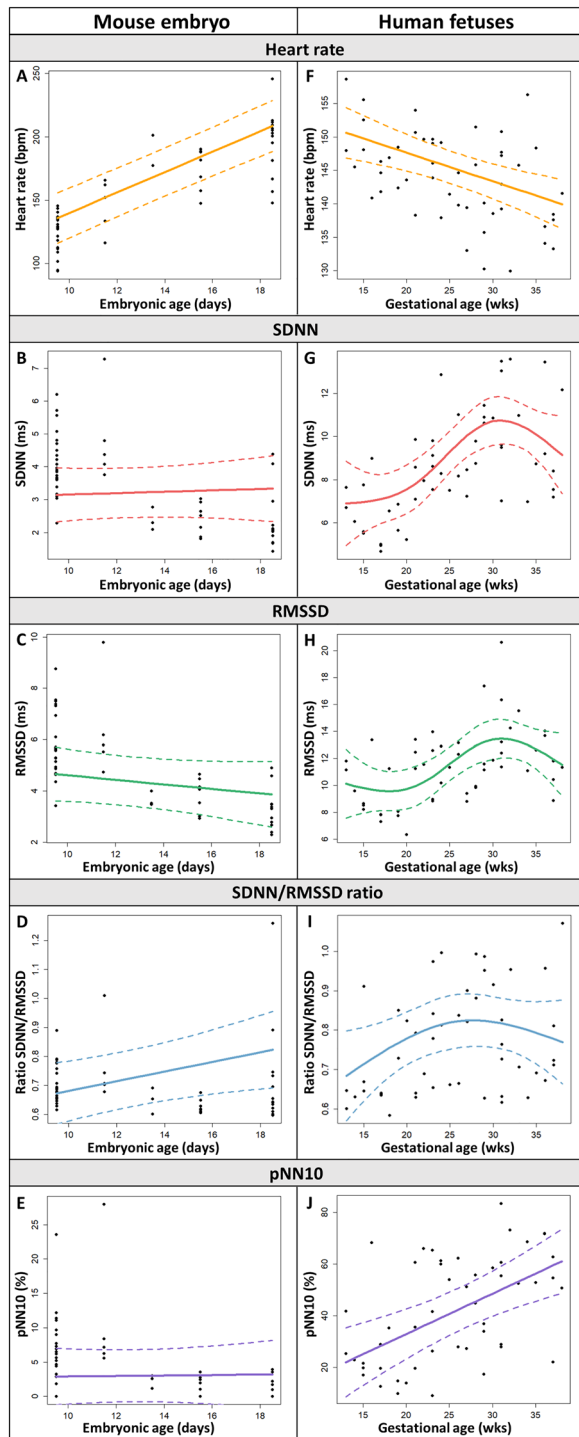


**Fig. 2** Examples of normal heart rhythm and ectopic heartbeats in wildtype mouse embryos. **A** Pulsed-wave Doppler tracing across the mitral and aortic valves showing normal heart rhythm at E18.5. During each cardiac cycle, there is a biphasic ventricular inflow pattern (E' and A') followed by a monophasic ventricular outflow pattern. **B** Pulsed-wave Doppler tracing at E13.5 showing multiple premature atrial contractions (PAC, yellow arrows), i.e. extrasystoles, all followed by compensatory pause [illustrated by the elongated passive filling phase (red arrows)]. **C** Pulsed-wave Doppler tracing at E18.5 showing a PAC followed by a tachycardia with a monophasic ventricular inflow pattern (only A'). E': passive ventricular inflow due to ventricular relaxation; A': active ventricular inflow due to atrial contraction; PAC: premature atrial contraction; S': ventricular outflow due to ventricular contraction



◀ **Fig. 3** Prenatal time trends of HRV parameters in murine and human embryos/fetuses. Time trends using linear mixed models corrected for mean embryonic/fetal heart rate and sex are provided separately for all HRV parameters. The dotted lines indicate 95% confidence intervals (CI) and the black dots indicate the raw data points. **A–E** HRV parameters in mouse embryos. **A** In mouse embryos, mean heart rate increased throughout gestation. **B, C** SDNN consistently low, whereas RMSSD demonstrated a slight decreasing trend. This suggests that, although a trend towards a decrease in parasympathetic activity during development was observed, definitive establishment of cardiac autonomic function is not yet observed. **D** The SDNN/RMSSD ratio remained predominant to RMSSD (i.e. ratio < 1), but increased in favor of SDNN throughout gestation. **E** pNN10 showed no specific trend. **F–J** HRV parameters in human fetuses. **F** In human fetuses, mean heart rate decreased throughout gestation. **G–H** SDNN and RMSSD increased from 20 to 30 WGA, suggesting that cardiac autonomic activity (mainly parasympathetic activity) establishes at approximately 20 WGA and matures until 30 WGA. **I** The SDNN/RMSSD ratio remained predominant to RMSSD (i.e. ratio < 1), demonstrating predominant vagal control throughout pregnancy. **J** pNN10 increased with gestation, which illustrates that vagal effect intensified throughout gestation. **F–J** are modified and extended after Zwanenburg et al. [30], published open access under Creative Commons Attribution License (CC BY)

addition, no difference was found in the number (first or second) of examination at onset (11/48 at first examination vs 11/24 at second examination,  $p=0.06$ ), eliminating a possible effect of previous anesthesia. In contrast to mice, the 48 eligible recordings of 18 human fetuses did not show cardiac ectopy or arrhythmias.

#### *Distinct prenatal dynamics in the development of cardiac autonomic function between mice and humans*

In mice, the remaining 50 study recordings without ectopic heartbeats were assessed by HRV analysis. In humans, 48 recordings were eligible for HRV analysis. The mean frame rate per second (fps) was 49.1 (18.3) in mice and 115 ( $\pm 27.1$ ) in humans, allowing heartbeats to be determined with respective precision levels of 0.02 s and 0.009 s. Time trends of all HRV parameters in mice and humans are provided in Fig. 3. Mean heart rate (HR) differed significantly throughout gestation between mice and humans ( $p < 0.01$ ): mean HR in mouse embryos increased from 136 ( $\pm 45.2$ ) to 208 ( $\pm 38.7$ ) beats/minute (linear trend  $R^2=0.699$ ,  $p \leq 0.0001$ ), whereas mean HR in human fetuses decreased from 149 ( $\pm 2.4$ ) to 138 ( $\pm 2.4$ ) beats/minute (linear trend  $R^2=0.231$ ,  $p=0.0005$ ). All other HRV parameters also showed differential time courses between mice and humans. In murine embryos, the SDNN (representing total heart rate variability) remained low and showed no particular trend [median 3.3 ms (IQR 2.15–4.25)]. Murine RMSSD (an indicator of vagal activity) displayed a slightly decreasing trend from 4.7 ms ( $\pm 2.4$ ) to 4.3 ms while the SDNN/RMSSD

(maternal respiratory rate 38.5 (IQR 34–43) vs 37.0 (IQR 36–45) breaths per minute,  $p=0.646$ ; maternal heart rate 540 (IQR 530–560) vs 535 (IQR 519.5–546.25) beats per minute,  $p=0.354$ ; and maternal temperature 36.2 (IQR 35.6–37.1) vs 36.6 (IQR 36.4–37.6) °C,  $p=0.131$ ). In

ratio increased, illustrating that the sympathovagal balance increased in favor of SDNN during gestation in mouse embryos. Murine pNN10, also demonstrating parasympathetic activity, remained consistently low at a median of 3.1% (IQR 1–7%). All these parameters in murine embryos together suggest that, although a minimal trend towards a decrease in parasympathetic activity during development was observed, definitive cANS function is not yet established prenatally in mice. In contrast, in humans, both SDNN and RMSSD increased evidently from approximately 20–30 WGA [SDNN 6.9 ms ( $\pm 1.3$ ) to 10.7 ms ( $\pm 0.7$ ); RMSSD 10.1 ms ( $\pm 1.7$ ) to 13.4 ms ( $\pm 1.0$ )] and showed a small decreasing trend thereafter, suggesting that cANS activity (mainly parasympathetic activity) is established prenatally around 20 WGA and the parasympathetic branch further matures until 30 WGA. In addition, the human SDNN/RMSSD ratio increased until 26 WGA, with predominance of RMSSD (i.e. ratio < 1) throughout pregnancy, indicating a predominant vagal tone. Human pNN10 showed a continuous linear increase from 13 to 38 WGA (22.0% ( $\pm 9.0$ ) to 60.0% ( $\pm 8.4$ ) [linear trend  $R^2 = 0.323$ ,  $p < 0.001$ ]), which illustrates that the vagal effect intensified throughout gestation.

#### **Morphological development of cardiac autonomic innervation in mice and humans**

To relate the results on cANS function to morphology, we next examined autonomic innervation and the contribution of NCCs as precursors thereof in murine and human heart specimens at sequential prenatal stages.

#### **Early cardiogenesis (mouse E9.5–E11.5, human 6–7 WGA): formation of the primary sympathetic chains and mediastinal vagal nerves**

*General morphology of the venous pole* During early cardiogenesis, cardiac structures at the venous pole are morphologically largely comparable between mice (E9.5–E11.5) and humans (6–7 WGA). In both species, the sinus venosus is well discernable as a U-shaped structure at the dorsal part of the common atrium, connected laterally to the left and right cardinal veins. At the entrance of the left and right cardinal veins, two putative SAN areas can be recognized as thickened clusters of cells (Fig. 4A–C, A'–C'). These SANs (i.e. a definitive right-sided and a transient left-sided SAN) become well established by E11.5 in mice. The vascular walls of the left and right cardinal veins are not yet covered by a myocardial sleeve and venous valves are not established in the early stages (until E11.5 in the mouse). The primordium of the pulmonary vein (the midpharyngeal endothelial strand (MPES)), is situated in the dorsal mesocardium and is initially not lumenized in both mice (E9.5–E10.5) and humans (6–7 WGA) (Fig. 4D,

D'). However, by E11.5 in mice, the primitive pulmonary vein shows a clear lumen and peripheral branches.

*Neural crest contributions* NCCs are similarly distributed in mice and humans during early cardiogenesis. By E9.5 in mice and 6 + 4 WGA in humans, neural crest(-derived) cells (Wnt1Cre-GFP<sup>+</sup> in mice and HNK-1<sup>+</sup> in humans) are prominently present in the regions of the primary sympathetic chains adjacent to the dorsal aortae (Fig. 4A, A', red arrows) and in the mesenchyme surrounding the foregut/developing oesophagus, which holds the area of the developing vagal nerves and developing parasympathetic cells (Fig. 4, blue arrows). NCCs are not discernable yet in the areas of the future parasympathetic cardiac ganglia in either species. Initially, the sinus venosus myocardium, SANs, proximal cardinal veins and MPES do not show expression of neural crest markers in mouse embryos of E9.5–E10.5 (Fig. 4A–D). However, at E11.5 in mice and 6 + 4 WGA in humans, neural crest(-derived) cells are first observed at the venous pole, although still in small numbers. They are present in the vicinity of the proximal part of the cardinal veins, in the dorsal mesocardium and sinus venosus myocardium near the MPES (Fig. 5A, A', blue arrowheads), and in mice also in the venous valves (not shown). However, no neural crest(-derived) cells are discerned yet in the area of the SANs.

*Autonomic nerve markers* Cardiac autonomic nerve markers follow a similar pattern during early cardiogenesis, with autonomic nerve development in the human embryo of 6–7 WGA closely resembling that of the E11.5 mouse embryo. By E10.5 in mice and at 6 + 4 WGA in humans, the sympathetic trunks have emerged bilaterally, staining positive for TUBB3, TH and ChAT (Fig. 5B–D, B'–D', red arrows). TUBB3<sup>+</sup> nerves are also identified in the area of the developing vagal nerves at this stage. In mice, these nerves initially still stain negative for TH and ChAT at E10.5, indicating that no differentiation towards a sympathetic or parasympathetic phenotype has occurred yet. By E11.5 in mice and 6 + 4 WGA in humans, these mediastinal nerves have differentiated towards a vagal phenotype, staining positive for ChAT with minimal co-expression of TH (Fig. 6B–D, B'–D', yellow arrows). No autonomic nerve markers are encountered yet in the area of the future parasympathetic cardiac ganglia. From E11.5 in mouse embryos and 6 + 4 WGA in the human embryo, the first TUBB3<sup>+</sup>/ChAT<sup>+</sup> nerves (i.e. parasympathetic nerves) are observed in the dorsal mesocardium near the developing pulmonary vein (Fig. 5B–C, B'–C', red arrowheads). Autonomic nerve markers are not observed in the sinus venosus myocardium, putative SAN areas or proximal cardinal veins during early cardiogenesis.

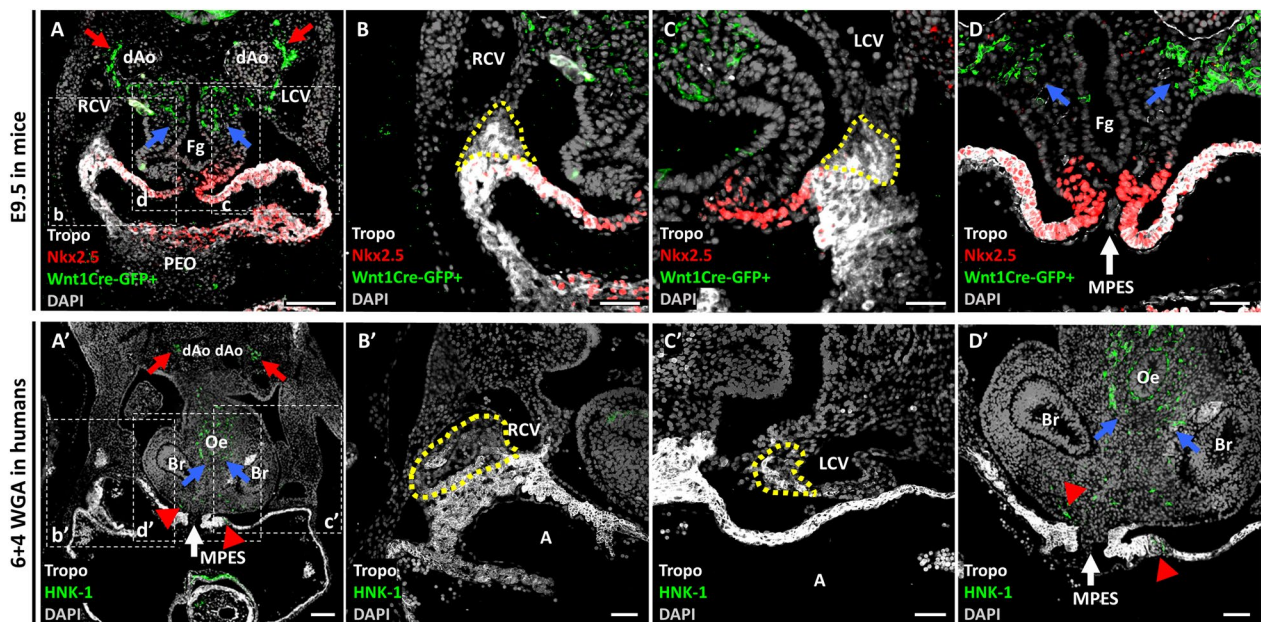


**Fig. 4** Neural crest cell distribution at early cardiogenesis (i.e. cardiac looping phase) in mice and humans. **A–D** Mouse sections at 9.5 depicting *Wnt1Cre-GFP<sup>+</sup>* neural crest lineage (green) cell distribution at the venous pole. The approximate location of **B–D** is indicated by the white dotted lines in **A**. Note **C** and **D** are from different sections. **A'–D'** Human sections at 6 + 4 WGA showing the distribution of HNK-1<sup>+</sup> (neural crest) cells (green) at the venous pole. The approximate location of **B'–D'** is indicated by the white dotted lines in **A'**. Note **D'** is from a different section. **A, A'** Overview sections in mice (**A**) and humans (**A'**). Note that in both species neural crest (-derived) cells are prominently present in the regions of the primary sympathetic chains adjacent to the dorsal aortae (red arrows) and in the mesenchyme surrounding the foregut where the parasympathetic cells and vagal nerves develop (blue arrows). Note also: endothelial cells (PECAM-1) are also stained in **A** (white). **B–C, B'–C'** At this early stage, no expression of neural crest cells (NCCs) is discerned in the putative right-sided sinoatrial node (SAN; yellow dotted line in **B, B'**) and left-sided SAN (**C, C'**; yellow dotted line). **D, D'** In mouse embryos of E9.5 (**D**), NCCs are not encountered in the area of the midpharyngeal endothelial strand (MPES), the precursor of the pulmonary vein. In the human embryo of 6 + 4 WGA (**D'**), HNK-1<sup>+</sup> neural crest cells are present in the dorsal mesocardium and sinus venosus myocardium nearby the MPES (red arrowheads). Blue arrows indicate NCCs at the area of the developing vagal nerves. Scalebars: A, A': 100  $\mu$ m, C, D, C', D': 50  $\mu$ m. A: common atrium; Br: pulmonary bronchus; dAo: dorsal aorta; Fg: foregut; L/RCV: left/right cardinal vein; MPES: mid-pharyngeal endothelial strand; Oe: oesophagus; PEO: proepicardial organ; SAN: sinoatrial node

#### **Mid-cardiogenesis (mouse E12.5–E13.5, human 8–9 WGA): autonomic nerve distribution at the venous pole of the heart**

**General morphology of the venous pole** During the next phase of cardiogenesis, the first differences in the area of the venous pole begin to emerge between mice (E12.5–13.5) and humans (8–9 WGA). The sinus venosus is initially in both species still U-shaped and connected laterally to the left and right cardinal veins, where formation of a myocardial sleeve is initiated. In mice, the sinus venosus still encompasses the definitive right-sided and the transient left-sided SAN, whereas in humans the left-sided SAN has disappeared by 8 WGA. Venous valves in the right atrium are well established at this stage in either species. The sinus venosus of murine embryos (E12.5–E13.5) maintains its symmetrical U-shape with ongoing development, although the sinus venosus myocardium becomes relatively smaller as the working atrial myocardium expands. In contrast, by 9 WGA in humans, the sinus venosus becomes lateralized to the right side as the lumen of the left superior cardinal vein has regressed. Its

remnant, the ligament of Marshall, can still be recognized, connected to the coronary sinus (Fig. 6). In both species, the primitive pulmonary vein has a clear lumen and peripheral branches, and formation of a myocardial sleeve is initiated (from E12.5 in mice and 8 WGA in humans) (Fig. 7).

**Neural crest contributions** Despite the anatomical differences at the venous pole, NCCs are similarly distributed in mouse and human during mid-cardiogenesis. By E12.5 in mice and 8 WGA in humans, the development of parasympathetic cardiac ganglia is discernable. Large clusters of neural crest(-derived) cells have formed adjacent to the myocardialized orifice of the primitive pulmonary vein (i.e. the developing parasympathetic cardiac ganglia), which merge with neural crest(-derived) clusters in the area of the vagal nerves (Fig. 7A, A'). In both species, neural crest(-derived) cells can now also be observed at all cardiac structures of the venous pole. Neural crest(-derived) cell tracts are present at most right-sided struc-

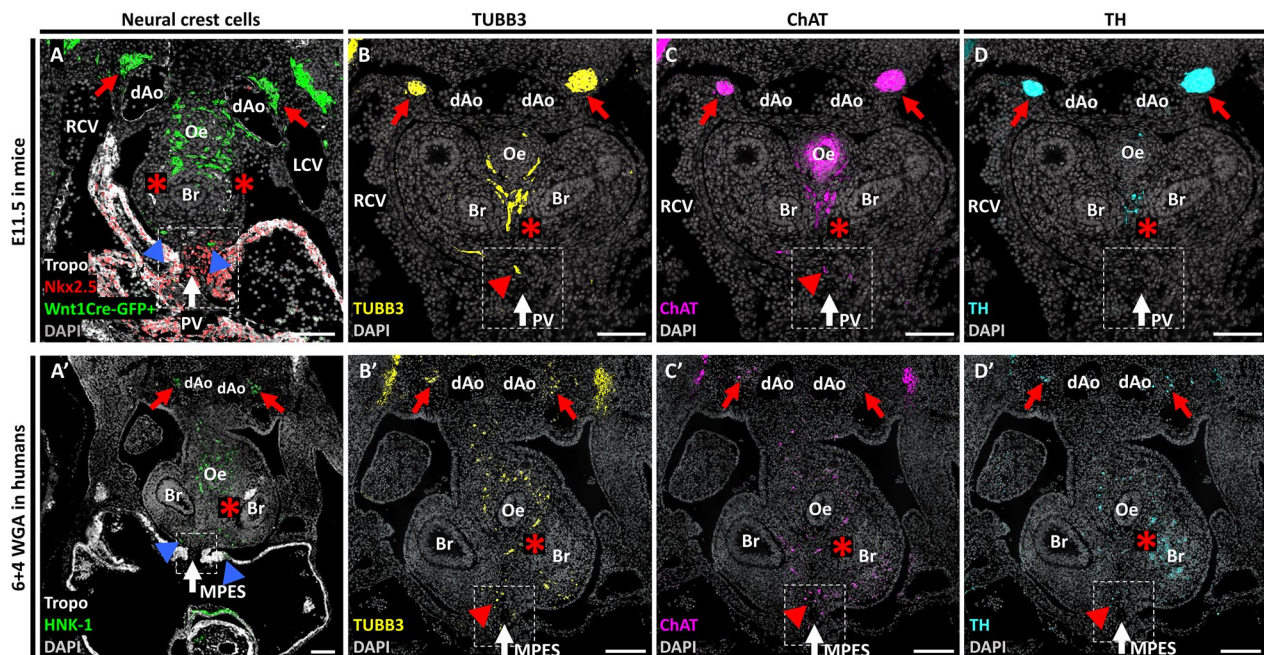


**Fig. 5** First parasympathetic nerves at the venous pole in proximity to the developing pulmonary vein in mice and humans. **A, A'** At E11.5 in mice (**A**) and 6+4 WGA in human (**A'**), a small number of neural crest(-derived) cells (*Wnt1Cre-GFP*<sup>+</sup> in mice and HNK-1<sup>+</sup> in humans) are encountered in the dorsal mesocardium and sinus venosus myocardium nearby the developing pulmonary vein (blue arrowheads). Also note the high amount of NCCs at the sympathetic chains (red arrows) and area of the vagal nerve (red asterisks). **B–D, B'–D'**. In both species, the sympathetic chains (red arrows) stain positive for TUBB3 (**B, B'**; yellow), ChAT (**C, C'**; magenta) and TH (**D, D'**; cyan). Also the vagal nerves have developed (red asterisks), staining positive for TUBB3 (**B, B'**) and ChAT (**C, C'**) with minimal co-expression of TH (**D, D'**). The first parasympathetic nerves are identified in the dorsal mesocardium nearby the developing pulmonary vein (red arrowheads), which stain positive for TUBB3 (**B, B'**) and ChAT (**C, C'**) but are negative for TH (**D, D'**). Scalebars: 100  $\mu$ m. Br: pulmonary bronchus; dAo: dorsal aorta; MPES: midpharyngeal endothelial strand; Oe: oesophagus; LCV/RCV: left/right cardinal vein; LV/RV: left/right ventricle; SAN: sinoatrial node; PV: pulmonary vein

tures of the venous pole [dorsal right atrial wall, the proximal right cardinal vein and the right-sided SAN (Fig. 8A, A')], while the venous valves are negative for NCC markers. Also left-sided structures of the venous pole (the coronary sinus, left proximal cardinal vein and the still unmyocardialized peripheral branches of the pulmonary vein) contain neural crest(-derived) cell tracts. In mice, a few NCCs are encountered in the transient left-sided SAN. Notably, when analyzing the embryos section by section, most NCC tracts at the venous pole, as well as a tract through the dorsal mesocardial protrusion to the area of the developing AV node, coalesce with the NCCs at the pulmonary venous ganglia (Fig. 7C, 7C'). By E13.5 in mice, the number of neural crest(-derived) cells at the venous pole has markedly increased. At this stage, additional large clusters of *Wnt1Cre-GFP*<sup>+</sup> cells have formed midposterior from the atria at a more cranial level than those surrounding the pulmonary vein, which are also found in the human embryo of 8 WGA.

**Autonomic nerve markers** As expected, cardiac autonomic nerves follow a similar pattern to neural crest(-derived) cells in both mice and humans, although the

timing of their differentiation varies between the two species relative to major cardiogenesis. From E12.5 in mice and 8 WGA in humans, the developing intrinsic ganglia surrounding the orifice of the primitive pulmonary vein stain positive for TUBB3 (Fig. 7B, B'). In mice, a few ganglion cells co-express ChAT and even fewer express TH, while the ganglia in humans lack autonomic nerve marker expression (Fig. 7B, B'). In both species, fine dispersed TUBB3<sup>+</sup> nerve fibers are observed between these ganglia and the dorsal right atrial wall, the coronary sinus and through the dorsal mesenchymal protrusion to the base of the atrial septum near the area of the developing AV node (Fig. 7D, D'). In mice, a small proportion of the nerves at the venous pole express ChAT, confirming previous observations that parasympathetic nerves arrive at the venous pole prior to sympathetic nerves [20]. In humans, all nerves are still undifferentiated, evidenced by the absence of ChAT and TH. At 8 WGA in humans, the first undifferentiated TUBB3<sup>+</sup> nerves are observed in the right-sided SAN (Fig. 8B'–D', red arrows). In contrast, at E12.5 in mice, no nerve fibers are encountered in both SANs. However, the right-sided SAN in mice features some

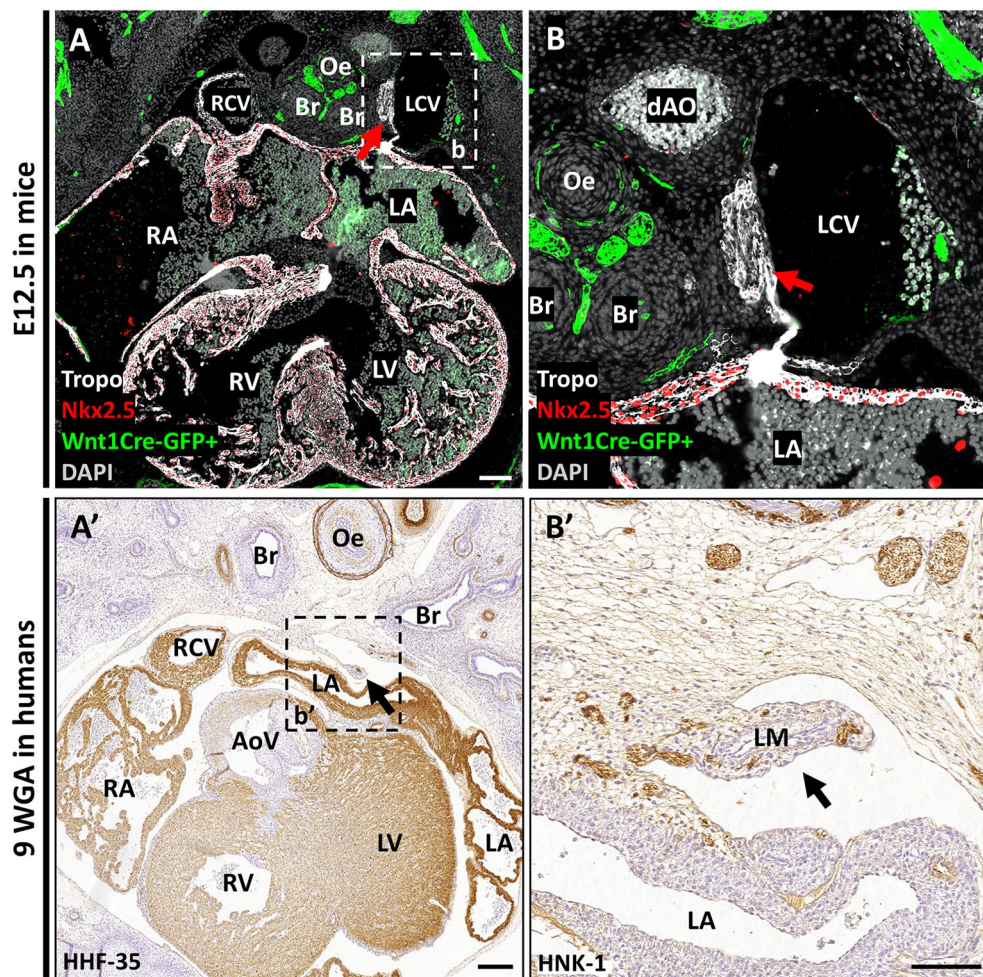


**Fig. 6** Anatomical differences at the venous pole at mid-cardiogenesis between mouse and human. **A, B** Mouse sections at E12.5 showing that the sinus venosus is connected laterally to the right- and left cardinal veins. Note that the transient left-sided SAN is still present at this stage (red arrow) and the myocardialization of the right cardinal vein is initiated. **A', B'** Human sections at 9 WGA depicting that the left superior cardinal vein has regressed. Its remnant, the ligament of Marshall (black arrow), is well discernable at this stage and shows high expression of HNK-1. Scalebars: 100  $\mu$ m. AoV: aortic valve; Br: pulmonary bronchus; dAo: dorsal aorta; LA/RA: left/right atrium; LCV/RCV: left/right cardinal veins; LM: Ligament of Marshall; LV/RV: left/right ventricle; Oe: oesophagus; SAN: sinoatrial node

TH<sup>+</sup>/TUBB3<sup>-</sup> cells, considered to be intrinsic cardiac adrenergic (ICA) cells [1], which increase in number with subsequent stages (Fig. 8D, yellow arrowheads). At stage E13.5 in mice, the cardiac ganglia highly express ChAT and faintly express TH. TUBB3<sup>+</sup>/ChAT<sup>+</sup> nerves extend further and are now present between the pulmonary venous ganglia and the right cardinal veins, both SANs, the coronary sinus and the pulmonary vein branches. The SANs contain both parasympathetic (ChAT<sup>+</sup>) and sympathetic (TH<sup>+</sup>) nerves (Fig. 8B–D, red arrows and arrowheads), while sympathetic nerves are sparse in the other structures at the venous pole.

#### **Late cardiogenesis (mouse E15.5–E18.5, human 10–20 WGA): spatial distribution and differentiation of cardiac autonomic nerves**

**General morphology of the venous pole** During late cardiogenesis, differences at the venous pole persist between mice (E15.5–18.5) and humans (10–20 WGA). In mice, both superior caval veins remain lumenized whereas only the right superior caval vein persists in humans. In both species, the caval vein(s) are fully covered by a myocardial sleeve at this stage. The definitive right-sided SAN has grown in size in either species, and the left-sided SAN in murine fetuses (which has already disappeared in human

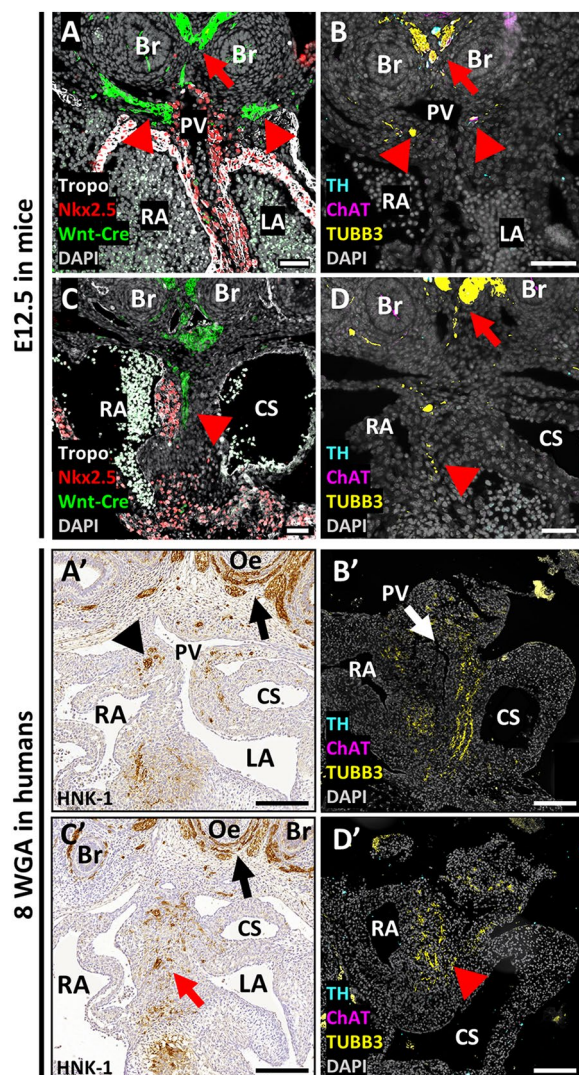


**Fig. 7** Neural crest and autonomic nerve markers surrounding the pulmonary vein and dorsal mesocardial protrusion in mouse and human at mid-cardiogenesis. **A–D** Mouse sections at E12.5. **A'–D'** Human sections at 8 WGA. **A, A'** Clusters of neural crest (-derived) cells (*Wnt1Cre-GFP*<sup>+</sup> in mice and HNK-1<sup>+</sup> in humans) surround the orifice of the pulmonary vein (PV), forming part of the intrinsic cardiac ganglia (red/black arrowheads). Note the vagal nerves surrounding the oesophagus (red arrow in **A** and black arrow in **A'**). **B, B'** The ganglia stain positive for TUBB3 (red arrowheads). Nerve stainings are depicted separately in Supplemental Fig. 2. In mice (**B**) most ganglion cells still only express TUBB3 (yellow), although a few ganglion cells co-express ChAT (magenta) and even fewer TH (cyan). Vagal nerves are indicated by the red arrows. In humans (**B'**), the nerves remain undifferentiated (only TUBB3 expression). **C, C'** Neural crest (-derived) cells at the dorsal mesenchymal protrusion between the PV clusters and the area of the developing atrioventricular (AV)-node (red arrow). **D, D'** In the same area, small TUBB3<sup>+</sup> nerves are present in both species, staining negative for TH and ChAT (red arrowheads). Nerve stainings are depicted separately in Supplemental Fig. 2. Scalebars: 50  $\mu$ m. Br: pulmonary bronchus; CS: coronary sinus; LA/RA: left/right atrium; Oe: Oesophagus; PV: pulmonary vein

embryos) has become fully incorporated into the myocardial sleeve surrounding the left superior caval vein. Venous valves are initially still present in both species. However, the venous valves have become indiscernible by 17 WGA in humans. The pulmonary veins in mouse embryos still drain via one solitary orifice, whereas in human fetuses, 4 separate orifices are visible. In both species, the myocardial sleeve covering the pulmonary veins is complete.

**Neural crest contributions** Lineage tracing in the mouse shows that neural crest-derived cells have increased in number and by E17.5, the expression pattern of *Wnt1Cre-GFP*<sup>+</sup> cells almost completely overlaps with TUBB3-expressing cells at all structures of the venous pole. In contrast, human HNK-1 expressed by migrating NCCs, has markedly decreased by 11 WGA. At that stage, there is only faint expression at the periphery of the SAN, the dorsal atrial wall, the area surrounding the pulmonary veins and at the mesocardial protrusion between the pulmonary ganglia and AV-junction.

**Autonomic nerve markers** During late cardiogenesis, the general development of the cANS is comparable between both species, but timing of autonomic differentiation (as reflected by expression patterns of TH and ChAT) differs relative to major cardiogenesis. In both species, a well-developed network of autonomic nerves at the venous pole has evolved (i.e. dorsal atrial wall, the superior caval vein(s), right-sided SAN and pulmonary veins) (Fig. 9) which gradually increases with ongoing gestation. In mouse embryos, the majority of TUBB3<sup>+</sup> at the venous pole now co-expresses ChAT and TH, although solely parasympathetic (TUBB3<sup>+</sup>/ChAT<sup>+</sup>) and sympathetic (TUBB3<sup>+</sup>/TH<sup>+</sup>) nerves are also found. In contrast, in human embryos, the first signs of differentiation are only encountered by 10 WGA. Similar to E12.5–E13.5 in mice, parasympathetic nerves are observed first, evidenced by the TUBB3<sup>+</sup>/ChAT<sup>+</sup>/TH<sup>-</sup> expression in the majority of ganglion cells and nerves. In addition, TUBB3<sup>+</sup> nerves lacking autonomic nerve markers are also still encountered. By 11 WGA, the first TH<sup>+</sup> cardiac ganglia and nerves are encountered at the venous pole. Notably, besides TH expression, they all co-express ChAT. Until 20 WGA, the majority of nerves and cardiac ganglia in human fetuses maintain predominant parasympathetic characteristics, although the proportion of nerves expressing TH increases. Most TH<sup>+</sup> nerves and ganglia retain their co-expression with ChAT. Notably, in both species, the number of both ChAT- and TH-expressing nerves in the definitive right-sided SAN also increases with gestation (from E13.5 in mice and 11WGA in humans). In mice, the number of TH<sup>+</sup>/TUBB3<sup>-</sup> cells, i.e. ICA cells, increases with ongo-

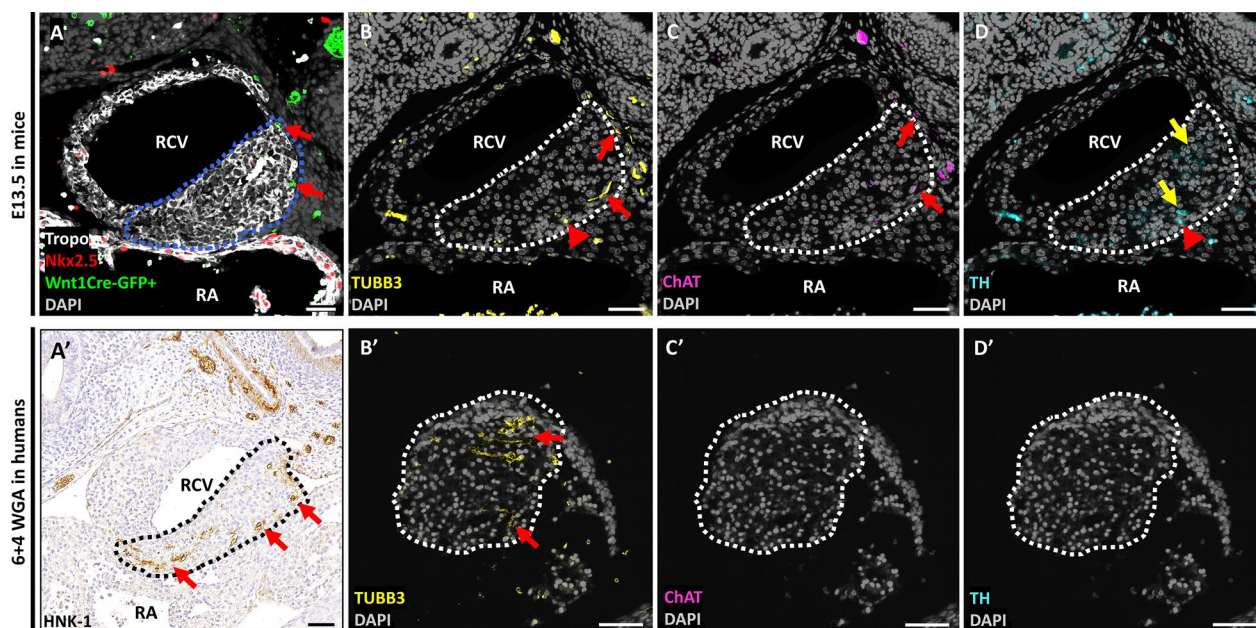


**Fig. 8** NCCs and autonomic nerve markers in the right-sided SAN in mice and humans at mid-cardiogenesis. **A–D** Mouse sections of the right-sided SAN (blue/white dotted line) at E13.5. **A'–D'** Human sections of the right-sided SAN (black/white dotted line) at 8WGA. **A, A'** In both species, neural crest(-derived) cells (*Wnt1Cre-GFP*<sup>+</sup> in mice and HNK-1<sup>+</sup> in humans) are present at the right-sided SAN (red arrows). **B, B'** In both species, TUBB3<sup>+</sup> nerves are found in the SAN (red arrows and arrowheads). **C–D, C'–D'** In mice, both parasympathetic [TUBB3<sup>+</sup>/ChAT<sup>+</sup>, red arrows in (B) and (C)] and sympathetic [TUBB3<sup>+</sup>/TH<sup>+</sup>, red arrowheads in (B) and (D)] nerves are present. Also note the ICA cells [TUBB3<sup>-</sup>/TH<sup>+</sup>, yellow arrowheads in (D)]. In human, the nerves remain undifferentiated [(red arrows in (B')), evidenced by the negative staining for ChAT (C') and TH (D')]. Scalebars: 50 μm. RA: right atrium; RCV: right cardinal vein

ing development whereas in the human SAN ICA cells are not present (Fig. 10).

All findings are summarized in Table 3.

## Discussion

The role of the cANS in outcome and late complications of cardiovascular diseases has increasingly been recognized over the past decades, in particular its role in the genesis and maintenance of atrial arrhythmias. Even in utero, proper functioning of the cANS has been shown to be an important indicator of fetal outcome [4, 37], and it has been postulated that (abnormal) prenatal development of the cANS might be related to cardiac autonomic dysfunction later in life [1]. Most of the pioneering studies providing insight into the embryological background of cANS development have been conducted in animal studies, whereas data derived from humans and how this compares to smaller mammals such as the mouse, is scarce. In the current study, we aimed to compare the morphological and functional cANS development between mouse and human embryos, specifically aimed at the venous pole, which harbors major predilection sites of atrial arrhythmias. Key findings of the current study are: (1) Prenatal function of the cANS differs greatly between the two species, as murine cANS function did

not appear to establish prior to birth while the dynamics of human cANS activation could be observed at 20 WGA and rapidly matured until 30 WGA. (2) Nerves reach the venous pole before autonomic function is established in both mice and humans. (3) Morphologically, the Anlage of the cANS follows a similar sequence in mice and humans. However, the timing of expression of sympathetic or parasympathetic markers differs when related to major cardiogenesis, with human cANS differentiation commencing relatively later. (4) Structures related to arrhythmogenicity, such as the ligament/vein of Marshall and the myocardium surrounding the caval and pulmonary veins, become highly innervated during embryonic development in both mice and humans, supporting a role of the cANS in modulation of focal arrhythmogenicity.

## Functional cANS development in mice and humans

In the current study, prenatal development of cANS function clearly differed between mice and humans. In mouse embryos, although the increase in heart rate and subtle decrease in RMSSD suggested a trend towards reduced parasympathetic tone, cANS function did not definitively establish in utero as no definitive trend of HRV parameters was observed. This contrasts with human fetuses, where a sudden increase in SDNN and

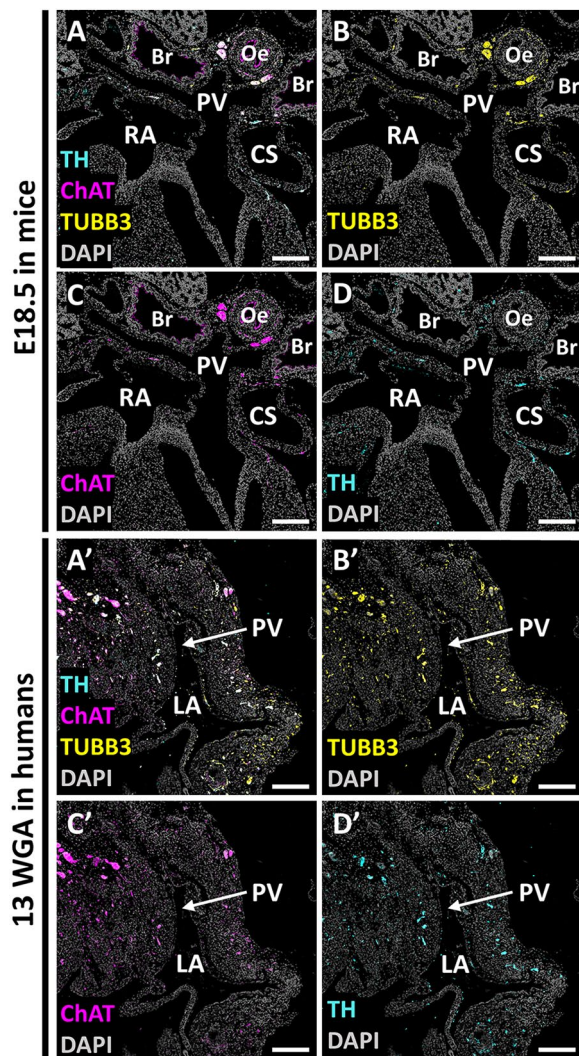


**Fig. 9** Autonomic nerve markers at the pulmonary vein in mice and humans at late cardiogenesis. **A–D** Mouse sections of the pulmonary vein at E18.5. The coronary sinus and dorsal right atrial wall with the orifice of the right superior caval vein and venous valves is also discernible. **A'–D'** Human sections of the pulmonary vein at 13 WGA. **A–D**. In mouse embryos at this stage, most nerves at the venous pole co-express both ChAT and TH. **A'–D'** Also in the human embryo of 13 WGA, many nerve cells co-express both ChAT and TH. Scalebars: 200 µm. Br: pulmonary bronchi; CS: coronary sinus; LA/RA: left/right atrium; LV/RV: left/right ventricle; Oe: oesophagus; PV: pulmonary vein

RMSSD from 20 to 30 WGA together with a decreased heart rate indicated that cANS function (mainly parasympathetic) establishes prenatally around 20 WGA and matures until 30 WGA. This discrepancy is not surprising given autonomic function also differs postnatally between species. Small adult rodents such as mice and rats generally exhibit a predominant sympathetic tone under standard laboratory conditions, while the

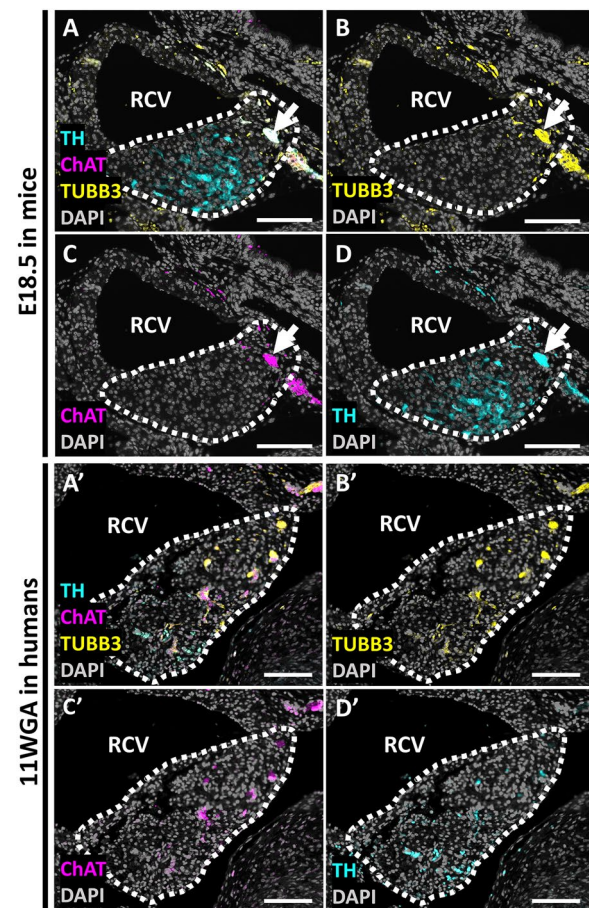


**Fig. 10** Autonomic nerve markers at the right-sided SAN in mice and humans during late cardiogenesis. **A–D** Mouse sections of the right-sided SAN (white dotted line) at E18.5. Large TUBB3<sup>+</sup> nerves are observed in the periphery of the SAN (white arrows), co-expressing both ChAT (**C**) and TH (**D**). Note the large amount of TH<sup>+</sup>/TUBB3<sup>-</sup> cells, i.e. ICA cells (**B** and **C**). **A'–D'** Human sections of the right-sided SAN (white dotted line) at 11 WGA. The SAN is highly innervated. Notably, the nerves are located more centrally compared to mice. ICA cells are not present. Scalebars: 100 µm. RCV: right cardinal vein

heart rate in larger mammals such as humans and sheep is mostly determined by vagal activity [12, 26]. Previous reports on prenatal cANS function in mouse embryos are very limited and comprise contrary results. Kasahara et al. reported an increase in heart rate only prior to birth, which was accompanied by a decrease in parasympathetic nervous activity while sympathetic activity remained unchanged [38]. The study of Khandoker et al. described an increasing heart rate together with an increasing trend of SDNN and RMSSD, suggesting that, in contrast to our study, cANS activity is already established prenatally in mouse embryos [39]. Notably, neither of these studies assessed HRV measurements

**Table 3** Similarities and differences in parallel stages of cANS development at the venous pole in mice and humans

Developmental stage	Major event general cardiogenesis	Similarities mouse-human	Differences mouse-human
Early cardiogenesis > Mice: E9.5–E11.5 > Human: 6–7 WGA	<ul style="list-style-type: none"> <li>• Cardiac looping</li> <li>• Sinus venosus U-shaped</li> <li>• Atrial septation initiated</li> </ul>	<ul style="list-style-type: none"> <li>• NCC migration</li> <li>• Sympathetic trunks and first mediastinal parasympathetic nerves discernable</li> <li>• TUBB3<sup>+</sup> cells in area of developing vagal nerves</li> <li>• NCCs in the dorsal mesocardium at the area of the developing PV</li> <li>• Absent parasympathetic cardiac ganglia</li> </ul>	
Mid cardiogenesis > Mice: E12.5–E13.5 > Human: 8–9 WGA	<ul style="list-style-type: none"> <li>• SAN formation established</li> <li>• Venous valves formed</li> <li>• Pulmonary vein canalized</li> <li>• Start myocardialization of cardinal vein(s) and pulmonary vein</li> </ul>	<ul style="list-style-type: none"> <li>• First TUBB3<sup>+</sup> nerves (co-expressing with ChAT) observed in the venous pole, entering near the developing PV</li> <li>• Cardiac ganglia formation at orifice pulmonary vein and dorsal atrial wall</li> <li>• TUBB3<sup>+</sup> nerves distribute over the (SAN(s), proximal cardinal vein(s), dorsal atrial wall, pulmonary vein</li> </ul>	<ul style="list-style-type: none"> <li>• Only in humans, the left SAN and left superior caval vein disappear</li> <li>• Only in mice, ICA cells appear in the right SAN</li> <li>• In humans nerves have not differentiated yet (ChAT and TH negative) while in mice most nerves are ChAT<sup>+</sup> and few TH<sup>+</sup></li> </ul>
Late cardiogenesis > Mice: E15.5–E18.5 > Human: 10–20 WGA	<ul style="list-style-type: none"> <li>• Major cardiogenesis is complete</li> </ul>	<ul style="list-style-type: none"> <li>• Increase of nerve distribution and density over venous pole</li> <li>• Most nerves express both TH and ChAT at later developmental stages</li> </ul>	<ul style="list-style-type: none"> <li>• In mice, the left-sided SAN disappears now</li> <li>• In mice, increase of ICA cells at the right-sided SAN, in human still absent</li> </ul>

longitudinally despite HRV showing large inter-individual differences [40]. Our data implies that murine cANS function presumably establishes after birth, which is supported by postnatal studies. HRV (SDNN and pNN6) is found to be low until postnatal day (P)4 in mouse pups, and only increased thereafter until 9 weeks of age [41]. In addition, neonatal mice developed a transient bradycardia as a stress response to attachment of electrocardiographic electrodes between P4–P8, which was attributed to the development of vagal activation [42]. Also for humans it is well known that further maturation of the human cANS occurs postnatally, as vagal activity reaches its maximum halfway through childhood and sympathetic activity continuously declines after birth [43]. Our finding that human cANS activity establishes prior to birth agrees with previous literature on this topic. However, studies show large variation for the trajectories of sympathetic and parasympathetic functional maturation, which is largely explained by differences in fetal state during HRV recording [30, 44–47]. Notably, despite the fairly large body of research on HRV development in human fetuses, it is essential to point out that fetal HRV has been assessed using a variety of techniques (such as fetal cardiocography, electrocardiography, magnetocardiography, and ultrasound) and analytical methods (i.e. time-domain analysis, frequency-domain analysis, Fast Fourier Transform, and Short-Time Fourier Transform), which makes direct comparisons between studies difficult and emphasizes the need for generic guidelines for human fetal HRV analysis [48].

#### Morphological cANS development in mice and humans

The current study demonstrated that although the Anlage of the cANS followed a similar developmental sequence, timing of differentiation into sympathetic or parasympathetic phenotype was markedly distinct between mice and humans (Table 3). The precursors of cardiac autonomic neurons, the NCCs, were in both species first observed in the dorsal mesocardium near the developing pulmonary vein (E9.5–11.5 in mice and 6–7 WGA in humans), and distributed from there over the venous pole with ongoing development (E12.5–E13.5 in mice and 8–9 WGA in humans). Similarly, Hildreth et al. observed Wnt1Cre-dependent  $\beta$ -galactosidase expression, indicative of neural crest cells, in the dorsal mesocardium of embryonic mice at E11.5 [22]. The arrival of neural crest cells at the heart has not been documented before in human embryos, but in chick embryos, another vertebrate species, NCCs also arrive at the venous pole, albeit at a later stage of cardiogenesis, HH32 [49]. Similar to NCCs and corresponding to previous literature, the first nerves reached the venous pole through the dorsal mesocardium bordering the pulmonary vein and developing interatrial septum at E12.5 in the mouse and 8–9 WGA in humans [22, 50]. In our study, timing of differentiation differed substantially between mice and humans in relation to major cardiogenesis. In the mouse, differentiation of cardiac nerves occurred during 4-chamber formation (nerves at the dorsal mesocardium are ChAT<sup>+</sup> and TH<sup>+</sup> at E12.5; atrial nerves are ChAT<sup>+</sup> at E12.5, and TH<sup>+</sup> at E13.5; nerves at the SAN are ChAT<sup>+</sup> and TH<sup>+</sup> by E13.5). Hildreth et al. also observed immunoreactivity

for TH and vesicular acetylcholine transporter, another parasympathetic marker in the dorsal mesocardium of mouse embryos at E12.5 [22], and Manousiouthakis et al. demonstrated the presence of TH<sup>+</sup> axons at the SAN in wildtype mice of E14 [51]. In contrast, in humans, differentiation emerged relatively later, when the heart had already achieved its final configuration (10 WGA for ChAT<sup>+</sup> atrial nerves, 11 WGA for TH<sup>+</sup> atrial nerves). Gordon et al. also reported a delay between the expression of general neural markers in the human SAN, at 8 WGA, and the expression of neuropeptides, at 10 WGA. TH immunoreactivity was also mostly limited to ganglia and paraganglia outside the heart until 10 WGA [52]. Of interest, we demonstrated that at late developmental stages in both mice and humans, many nerves co-express ChAT and TH. This may represent a transient state during embryonic development related to PHOX2B expression [53]. However, this explanation is not all-encompassing, as adult autonomic neurons retain the ability to switch phenotypes in response to disease states, such as during heart failure, after myocardial infarction, or following sympathectomy [12, 54]. Co-expression of cholinergic and catecholaminergic neurotransmitters may therefore represent a compensatory mechanism. Finally, it may reflect a 'dual-transmitter' phenotype, as has been described for other neurons [55], supporting the notion of a more nuanced neurotransmitter profile than has classically been appreciated for the cANS.

#### Functional versus morphological cANS development

In this study, establishment of cANS function did not directly relate to morphological development of autonomic nerves, as autonomic innervation was observed substantially earlier at sinus venosus-related structures including the SAN. Interestingly, the heart rate in both species already showed a clear alteration before cANS function had been established. It is known that the embryonic heart rate already responds to catecholamines prior to establishment of cANS innervation [56]. ICA cells, the major source of early catecholamine synthesis, have been suggested as an underlying mechanism [1, 57]. In our study, ICA cells were observed in mice from E12.5, which increased in number with subsequent developmental stages, while the human SAN did not contain ICA cells. The epicardium may also play a role in early autonomic function of the heart, as mechanical epicardial inhibition disturbs the response to catecholamines in chick embryos [58]. Remarkably, severe epicardial inhibition in the sinus venosus area resulted in a more pronounced effect than mild inhibition in the same area. Autonomic nerve markers and adrenergic beta receptors are expressed in both mouse and human epicardium,

although the functional meaning of this finding is still largely unexplored [58].

#### Autonomic innervation and clinical arrhythmias

Autonomic imbalance is associated with the occurrence of atrial arrhythmias [10, 59]. Electrophysiological studies have shown that the majority of atrial arrhythmias originate from sinus venosus-related structures [13]. Notably, in adults these structures tend to be more densely innervated compared to other regions of the atrium [2]. The ligament/vein of Marshall has complex nervous connections to the coronary sinus and orifices of the pulmonary veins, which are related to the genesis of atrial fibrillation [60]. In addition, the area surrounding the pulmonary venous myocardium contains numerous ganglionated plexuses that can trigger atrial fibrillation when stimulated [59, 61]. The current study shows that the inflow tract myocardium at the venous pole becomes highly innervated during embryonic development. Notably, not only the definitive right-sided SAN and myocardium of the right cardinal vein (primordium of the superior caval vein), but also a transient left-sided SAN and the myocardium of the left cardinal vein (which regresses in humans to become the ligament of Marshall), as well as the myocardium surrounding the pulmonary veins, are highly innervated at early gestation. These findings may potentially explain a modulatory role of the cANS in focal arrhythmogenicity originating from structures such as the ligament of Marshall and the pulmonary veins, under pathological conditions [13, 14]. It remains unclear at this point what the function of the broad autonomic innervation of the venous pole myocardium is. We and others have previously shown that the fetal cardiac conduction system initially comprises a broad area with pacemaker activity (corresponding to the sinus venosus myocardium), potentially explaining why cardiac innervation follows this broad pattern [19, 62]. Another hypothesis is that the sinus venosus guides nerve sprouting, as was shown for sympathetic axons in mouse embryos [51].

#### Prenatal atrial ectopy in relation to autonomic innervation of the venous pole

We demonstrated frequently occurring ectopic heart beats in mice embryos, which remarkably coincided with the onset of SAN innervation, and with the right-sided lateralization of the initially broad Anlage of the embryonic CCS [16–18]. Although ectopic beats were not observed in human fetuses in the current study, atrial ectopy is a regular finding in the prenatal period [63]. The cause of these ectopic beats is still debated, but the apparent association with the start of SAN innervation

and CCS/sinus venosus lateralization invites speculation that prenatal atrial ectopy marks a transition phase in SAN autonomic regulation and function.

### Limitations and considerations

Regarding cANS function, it should be noted that functional measurements in mouse embryos were obtained while the mother mice were sedated with isoflurane anesthesia, whereas the human data were retrieved without anesthetics. Low-dose isoflurane as used in this study, however, has only minimal effect on the autonomic reflexes of adult mice, as evidenced by the variations in maternal heart rate and respiratory rate. Therefore, the effect on mouse embryos is presumed to be marginal. Conducting ultrasound recordings without anesthetics is highly stressful for the mother mice and is therefore not feasible. Regarding cANS morphology, human fetal specimens for biomedical research are relatively scarce, and the number of specimens included in this study was dictated by the availability of fetal human specimens in our biobanks. In addition, lineage tracing, which provides valuable insights into cellular origin, development and differentiation in mouse embryos, is not feasible in human fetuses. Nevertheless, to the best of our knowledge, this is the first study that provides a comparative timeline of prenatal cANS development in humans and mice, encompassing both functional and morphological aspects, offering valuable insights within the constraints of available resources.

### Conclusions and future perspectives

This study shows that, although the early morphological cANS development at the venous pole follows a similar sequence, there are substantial differences between mice and humans. Anatomically, the timing of differentiation into sympathetic or parasympathetic phenotype differs in relation to major cardiogenesis, with human autonomic markers emerging relatively later. Functionally, however, the human fetal cANS (mainly parasympathetic) becomes activated around 20 WGA and matures until 30 WGA, whereas full murine cANS activity is not yet established in mouse embryos. These results should be taken into account when extrapolating mouse studies of the cANS to humans. In particular, mouse embryos likely do not replicate the cANS observed during advanced gestation in humans. In both mice and humans, structures related to arrhythmogenicity in human, such as the ligament of Marshall and the myocardium surrounding the pulmonary veins, become highly innervated during embryonic development, potentially explaining a modulatory role of the cANS in focal arrhythmogenicity under pathological

conditions. Current promising techniques such as the use of single-cell RNA sequencing, disease modelling using human induced pluripotent stem cells or computational modelling, may help to further unravel the mechanisms and involved pathways of human cANS development and its potential role in arrhythmogenesis later in life.

### Abbreviations

cANS	Cardiac autonomic nervous system
ChAT	Choline o-acetyltransferase
cTDI	Color Tissue Doppler Imaging
eGFP	Enhanced green fluorescent protein
E	Embryonic day
Fps	Frames per second
HR	Heart rate
HCN4	Hyperpolarization activated cyclic nucleotide gated potassium channel 4
HNK-1	Human natural killer-1
HRV	Heart rate variability
ICA cells	Intrinsic cardiac adrenergic cells
MPES	Midpharyngeal endothelial strand
NCCs	Neural crest cells
P	Postnatal day
PHOX2B	Paired like homeobox 2B
pNN10	Proportion of normal-to-normal beat intervals differing more than 10 ms
RMSSD	Root mean square of successive differences between normal-to-normal beats
SAN	Sinoatrial node
SDNN	Standard deviation of all normal-to-normal interbeat intervals
TH	Tyrosine hydroxylase
TUBB3	Tubulin beta 3 class III
WGA	Weeks gestational age

### Supplementary Information

The online version contains supplementary material available at <https://doi.org/10.1186/s12967-024-06049-y>.

Supplementary Material 1: Supplemental Figure 1 - Schematic representation of the study design. A: common atrium, Ao: aorta, AoS: aortic sac, CCS: cardiac conduction system, CS: coronary sinus, E: embryonic day, GCV: great cardiac vein, HRV: heart rate variability, I/SVC: inferior/superior caval vein, L/RA: left/right atrium, L/RVC: left/right cardinal vein, L/RV: left/right ventricle, PV: pulmonary vein, PT: pulmonary trunk, RR: interbeat interval, SAN: sinoatrial node, SHF: second heart field, V: common ventricle, VM: vein of Marshall/Marshall ligament, VV: venous valves, WGA: weeks gestational age, WT: wildtype. Panel B is modified after Zwanenburg et al. [30], schematic drawings dorsal view are modified after Jongbloed et al. [18], with copyright 2023 from Copyright Clearance Center.

Supplementary Material 2: Supplemental Figure 2 - Autonomic nerve markers surrounding the pulmonary vein and dorsal mesocardial protrusion. A-D. Mouse sections at E12.5 depicting autonomic nerve markers surrounding the orifice of the pulmonary vein. Vagal nerves are indicated by the red arrow. E-H. Mouse sections at E12.5 depicting autonomic nerve markers at the dorsal mesenchymal protrusion between the PV clusters and the area of the developing atrioventricular-node. Vagal nerves are indicated by the red arrow. Scalebars: 50µm. Br: pulmonary bronchus, CS: coronary sinus, LA/RA: left/right atrium, PV: pulmonary vein.

### Acknowledgements

The authors gratefully thank Ronald Slagter for the illustration of Fig. 1 in this manuscript. In addition, we greatly acknowledge the large contribution of dr. A.R.H. Twijnstra in the setup of the local biobank "Ectopic pregnancy", which provides valuable material for studying early embryonic development. We

thank Dr. Joshua Peterson for his work in creating the murine Wnt1Cre;mT/mG lineage tracing models.

#### Author contributions

Conceptualization and design: F.Z. and M.R.M.J. Experiments: F.Z., L.J.W., C.J.M. Analysis and interpretation of the data: F.Z., M.R.M.J., T.A.B., A.D.J.H. Critical revision for intellectual content: T.A.B., A.D.J.H., M.H., N.D.H., R.E.P., N.A.B., M.C.dR, M.R.M.J. All authors agree to be accountable for all aspects of their work and gave final approval of the manuscript to be published.

#### Funding

M.R.M.J. is supported by a personal research grant from NWO ZonMw (projectnr. 91719346) and by a Rembrandt grant. M.C.dR. and M.R.M.J. are supported by a grant of the Dutch Bontius Foundation. M.C.dR is supported by the Netherlands Heart Foundation (project number 2019B002 OUTREACH).

#### Data availability

The data underlying this article will be shared on reasonable request to the corresponding author.

#### Declarations

##### Ethics approval and consent to participate

Mouse experiments were approved by the local animal welfare committee of the Leiden University Medical Center (# AVD1160020185325) and performed in accordance with the Guide for Care and Use of Laboratory Animals as published by the NIH (57). Human experiments were approved by the Medical Ethical Committee of the Leiden University Medical Center (# NL65087.058.18) and Biobank of Ectopic pregnancy (#B19.060), with all participants providing written informed consent. Historical material was collected according to contemporary rules and regulations in compliance with rules and regulations for the proper use of human tissues for scientific research and is part of the institutional biobank (# B21.051).

##### Consent for publication

Not applicable.

##### Competing interests

The authors report no conflict of interest. The funders had no role in the design of the study; in the collection, analyses, or interpretation of data; in the writing of the manuscript, or in the decision to publish the results.

##### Author details

<sup>1</sup>Department of Obstetrics and Fetal Medicine, Leiden University Medical Center, Leiden, The Netherlands. <sup>2</sup>Department of Anatomy & Embryology, Leiden University Medical Center, P.O. Box 9600, Postal Zone: S-1-P, 2300 RC Leiden, The Netherlands. <sup>3</sup>Department of Pediatric Cardiology, Leiden University Medical Center, Leiden, The Netherlands. <sup>4</sup>Institute of Biology, Leiden University, Leiden, The Netherlands. <sup>5</sup>Department of Cardiology, Leiden University Medical Center, Leiden, The Netherlands. <sup>6</sup>Center of Congenital Heart Disease Amsterdam-Leiden (CAHAL), Leiden, The Netherlands.

Received: 28 August 2024 Accepted: 25 December 2024

Published online: 15 January 2025

#### References

- Végh AMD, Duim SN, Smits AM, Poelmann RE, Ten Harkel ADJ, DeRuiter MC, Goumans MJ, Jongbloed MRM. Part and parcel of the cardiac autonomic nerve system: unravelling its cellular building blocks during development. *J Cardiovasc Dev Dis.* 2016;3:28.
- Zandstra TE, Notenboom RGE, Wink J, Kiës P, Vliegen HW, Egorova AD, Schalij MJ, De Ruiter MC, Jongbloed MRM. Asymmetry and heterogeneity: part and parcel in cardiac autonomic innervation and function. *Front Physiol.* 2021;12:665298.
- Shaw CJ, Allison BJ, Itani N, Botting KJ, Niu Y, Lees CC, Giussani DA. Altered autonomic control of heart rate variability in the chronically hypoxic fetus. *J Physiol.* 2018. <https://doi.org/10.1113/JP275659>.
- Schnettler WT, Goldberger AL, Ralston SJ, Costa M. Complexity analysis of fetal heart rate preceding intrauterine demise. *Eur J Obstet Gynecol Reprod Biol.* 2016;203:286–90.
- Moon RY, Horne RS, Hauck FR. Sudden infant death syndrome. *Lancet.* 2007;370:1578–87.
- Li CY, Li YG. Cardiac sympathetic nerve sprouting and susceptibility to ventricular arrhythmias after myocardial infarction. *Cardiol Res Pract.* 2015;2015:698368.
- Diller GP, Dimopoulos K, Okonko D, Uebing A, Broberg CS, Babu-Narayan S, Bayne S, Poole-Wilson PA, Sutton R, Francis DP, Gatzoulis MA. Heart rate response during exercise predicts survival in adults with congenital heart disease. *J Am Coll Cardiol.* 2006;48:1250–6.
- Chen HS, Voortman LM, van Munsteren JC, Wisse LJ, Tofig BJ, Kristiansen SB, Glashan CA, DeRuiter MC, Zeppenfeld K, Jongbloed MRM. Quantification of large transmural biopsies reveals heterogeneity in innervation patterns in chronic myocardial infarction. *JACC Clin Electrophysiol.* 2023;9:1652–64.
- Hillebrand S, Gast KB, de Mutsert R, Swenne CA, Jukema JW, Middeldorp S, Rosendaal FR, Dekkers OM. Heart rate variability and first cardiovascular event in populations without known cardiovascular disease: meta-analysis and dose-response meta-regression. *Europace.* 2013;15:742–9.
- Shen MJ, Zipes DP. Role of the autonomic nervous system in modulating cardiac arrhythmias. *Circ Res.* 2014;114:1004–21.
- Zandstra T, Kiës P, Maan A, Man SC, Bootsma M, Vliegen H, Egorova A, Mertens B, Holman E, Schalij M, Jongbloed M. Association between reduced heart rate variability components and supraventricular tachyarrhythmias in patients with a systemic right ventricle. *Auton Neurosci.* 2020;227:102696.
- Hasan W. Autonomic cardiac innervation: development and adult plasticity. *Organogenesis.* 2013;9:176–93.
- Kistler PM, Roberts-Thomson KC, Haqqani HM, Fynn SP, Singarayay S, Vohra JK, Morton JB, Sparks PB, Kalman JM. P-wave morphology in focal atrial tachycardia: development of an algorithm to predict the anatomic site of origin. *J Am Coll Cardiol.* 2006;48:1010–7.
- Haïssaguerre M, Jais P, Shah DC, Takahashi A, Hocini M, Quiniou G, Garrigue S, Le Mouroux A, Le Métayer P, Clémenty J. Spontaneous initiation of atrial fibrillation by ectopic beats originating in the pulmonary veins. *N Engl J Med.* 1998;339:659–66.
- He B, Wang X, Zhao F, Guo T, Po SS, Lu Z. The ligament of Marshall and arrhythmias: a review. *Pacing Clin Electrophysiol.* 2021;44:792–9.
- Vicente-Steijn R, Passier R, Wisse LJ, Schalij MJ, Poelmann RE, Gittenberger-de Groot AC, Jongbloed MR. Funny current channel HCN4 delineates the developing cardiac conduction system in chicken heart. *Heart Rhythm.* 2011;8:1254–63.
- Vicente-Steijn R, Kolditz DP, Mahtab EA, Askar SF, Bax NA, Van Der Graaf LM, Wisse LJ, Passier R, Pijnappels DA, Schalij MJ, et al. Electrical activation of sinus venosus myocardium and expression patterns of RhoA and Isl-1 in the chick embryo. *J Cardiovasc Electrophysiol.* 2010;21:1284–92.
- Jongbloed MR, Vicente Steijn R, Hahurij ND, Kelder TP, Schalij MJ, Gittenberger-de Groot AC, Blom NA. Normal and abnormal development of the cardiac conduction system; implications for conduction and rhythm disorders in the child and adult. *Differentiation.* 2012;84:131–48.
- Rivaud MR, Blok M, Jongbloed MRM, Boukens BJ. How cardiac embryology translates into clinical arrhythmias. *J Cardiovasc Dev Dis.* 2021;8:70.
- Hildreth V, Anderson RH, Henderson DJ. Autonomic innervation of the developing heart: origins and function. *Clin Anat.* 2009;22:36–46.
- Verberne ME, Gittenberger-de Groot AC, Poelmann RE. Lineage and development of the parasympathetic nervous system of the embryonic chick heart. *Anat Embryol.* 1998;198:171–84.
- Hildreth V, Webb S, Bradshaw L, Brown NA, Anderson RH, Henderson DJ. Cells migrating from the neural crest contribute to the innervation of the venous pole of the heart. *J Anat.* 2008;212:1–11.
- Kirby ML, McKenzie JW, Weidman TA. Developing innervation of the chick heart: a histofluorescence and light microscopic study of sympathetic innervation. *Anat Rec.* 1980;196:333–40.
- Pauza DH, Skripka V, Pauziene N, Stropus R. Morphology, distribution, and variability of the epicardial neural ganglionated subplexuses in the human heart. *Anat Rec.* 2000;259:353–82.
- Aksu T, Gopinathannair R, Gupta D, Pauza DH. Intrinsic cardiac autonomic nervous system: what do clinical electrophysiologists need to know about the "heart brain"? *J Cardiovasc Electrophysiol.* 2021;32:1737–47.

26. MacDonald EA, Rose RA, Quinn TA. Neurohumoral control of sinoatrial node activity and heart rate: insight from experimental models and findings from humans. *Front Physiol.* 2020;11:170.
27. Hahurij ND, Calkoen EE, Jongbloed MR, Roest AA, Gittenberger-de Groot AC, Poelmann RE, De Ruiter MC, van Munsteren CJ, Steendijk P, Blom NA. Echocardiographic assessment of embryonic and fetal mouse heart development: a focus on haemodynamics and morphology. *ScientificWorldJournal.* 2014;2014:531324.
28. TFCNASP Electrophysiology. Heart rate variability: standards of measurement, physiological interpretation and clinical use. Task Force of the European Society of Cardiology and the North American Society of Pacing and Electrophysiology. *Circulation.* 1996;93:1043–65.
29. Eschbach SJ, Gijtenbeek M, van Geloven N, Oepkes D, Haak MC. Measurement of cardiac function by cardiac time intervals, applicability in normal pregnancy and twin-to-twin transfusion syndrome. *J Echocardiogr.* 2019;17:129–37.
30. Zwanenburg F, Jongbloed MRM, van Geloven N, Ten Harkel ADJ, van Lith JMM, Haak MC. Assessment of human fetal cardiac autonomic nervous system development using color tissue Doppler imaging. *Echocardiography.* 2021;38:974–81.
31. Mahtab EA, Vicente-Steijn R, Hahurij ND, Jongbloed MR, Wisse LJ, DeRuiter MC, Uhrin P, Zujec J, Binder BR, Schalijs MJ, et al. Podoplanin deficient mice show a RhoA-related hypoplasia of the sinus venosus myocardium including the sinoatrial node. *Dev Dyn.* 2009;238:183–93.
32. Peterson JC, Chughtai M, Wisse LJ, Gittenberger-de Groot AC, Feng Q, Goumans MTH, VanMunsteren JC, Jongbloed MRM, DeRuiter MC. Bicuspid aortic valve formation: Nos3 mutation leads to abnormal lineage patterning of neural crest cells and the second heart field. *Dis Model Mech.* 2018;11:dmm034637.
33. Gittenberger-de Groot AC, Peterson JC, Wisse LJ, Roest AAW, Poelmann RE, Bökenkamp R, Elzenga NJ, Hazekamp M, Bartelings MM, Jongbloed MRM, DeRuiter MC. Pulmonary ductal coarctation and left pulmonary artery interruption; pathology and role of neural crest and second heart field during development. *PLoS ONE.* 2020;15: e0228478.
34. Blom NA, Gittenberger-de Groot AC, DeRuiter MC, Poelmann RE, Mentink MM, Ottenkamp J. Development of the cardiac conduction tissue in human embryos using HNK-1 antigen expression: possible relevance for understanding of abnormal atrial automaticity. *Circulation.* 1999;99:800–6.
35. Tucker GC, Delarue M, Zada S, Boucaut JC, Thiery JP. Expression of the HNK-1/NC-1 epitope in early vertebrate neurogenesis. *Cell Tissue Res.* 1988;251:457–65.
36. Betteres E, Liu Y, Kjaeldgaard A, Sundström E, García-Castro MI. Analysis of early human neural crest development. *Dev Biol.* 2010;344:578–92.
37. Practice bulletin no. 145: antepartum fetal surveillance. *Obstet Gynecol.* 2014;124:182–92.
38. Kasahara Y, Yoshida C, Saito M, Kimura Y. Assessments of heart rate and sympathetic and parasympathetic nervous activities of normal mouse fetuses at different stages of fetal development using fetal electrocardiography. *Front Physiol.* 2021;12:652828.
39. Khandoker AH, Al Khoori T, Ito T, Sugibayashi R, Kimura Y. Assessment of autonomic neurodevelopment in the mouse fetuses by using fetal electrocardiography. *Annu Int Conf IEEE Eng Med Biol Soc.* 2016;2016:2954–7.
40. Van Leeuwen P, Cysarz D, Edelhäuser F, Grönemeyer D. Heart rate variability in the individual fetus. *Auton Neurosci.* 2013;178:24–8.
41. Heier CR, Hampton TG, Wang D, Didonato CJ. Development of electrocardiogram intervals during growth of FVB/N neonate mice. *BMC Physiol.* 2010;10:16.
42. Sato S. Quantitative evaluation of ontogenetic change in heart rate and its autonomic regulation in newborn mice with the use of a noninvasive piezoelectric sensor. *Am J Physiol Heart Circ Physiol.* 2008;294:H1708–1715.
43. Hartevelde LM, Nederend I, Ten Harkel ADJ, Schutte NM, de Rooij SR, Vrijkotte TGM, Oldenhof H, Popma A, Jansen LMC, Suurland J, et al. Maturation of the cardiac autonomic nervous system activity in children and adolescents. *J Am Heart Assoc.* 2021;10: e017405.
44. Schneider U, Bode F, Schmidt A, Nowack S, Rudolph A, Doelcker EM, Schlattmann P, Gotz T, Hoyer D. Developmental milestones of the autonomic nervous system revealed via longitudinal monitoring of fetal heart rate variability. *PLoS ONE.* 2018;13: e0200799.
45. Schneider U, Frank B, Fiedler A, Kaehler C, Hoyer D, Liehr M, Hauelsen J, Schlessner E. Human fetal heart rate variability-characteristics of autonomic regulation in the third trimester of gestation. *J Perinat Med.* 2008;36:433–41.
46. Brändle J, Preissl H, Draganova R, Ortiz E, Kagan KO, Abele H, Brucker SY, Kiefer-Schmidt I. Heart rate variability parameters and fetal movement complement fetal behavioral states detection via magnetography to monitor neurovegetative development. *Front Hum Neurosci.* 2015;9:147.
47. Mannella P, Billeci L, Giannini A, Canu A, Pancetti F, Simoncini T, Varanini M. A feasibility study on non-invasive fetal ECG to evaluate prenatal autonomic nervous system activity. *Eur J Obstet Gynecol Reprod Biol.* 2020;246:60–6.
48. Ponsiglione AM, Cosentino C, Cesarelli G, Amato F, Romano M. A comprehensive review of techniques for processing and analyzing fetal heart rate signals. *Sensors.* 2021;21:6136.
49. Poelmann RE, Gittenberger-de Groot AC. A subpopulation of apoptosis-prone cardiac neural crest cells targets to the venous pole: multiple functions in heart development? *Dev Biol.* 1999;207:271–86.
50. Golub DM, Loyko RM, Novikov II. Development of reflexogenic zone innervation of the human cardiovascular system. *Anat Anz.* 1979;145:474–92.
51. Manousiouthakis E, Mendez M, Garner MC, Exertier P, Makita T. Venous endothelin guides sympathetic innervation of the developing mouse heart. *Nat Commun.* 2014;5:3918.
52. Gordon L, Polak JM, Moscoso GJ, Smith A, Kuhn DM, Wharton J. Development of the peptidergic innervation of human heart. *J Anat.* 1993;183(Pt 1):131–40.
53. Ernsberger U, Rohrer H. Sympathetic tales: subdivisions of the autonomic nervous system and the impact of developmental studies. *Neural Dev.* 2018;13:20.
54. Ge Y, van Roon L, van Gils JM, Geestman T, van Munsteren CJ, Smits AM, Goumans M, DeRuiter MC, Jongbloed MRM. Acute myocardial infarction induces remodeling of the murine superior cervical ganglia and the carotid body. *Front Cardiovasc Med.* 2022;9:758265.
55. Vaaga CE, Borisovska M, Westbrook GL. Dual-transmitter neurons: functional implications of co-release and co-transmission. *Curr Opin Neurobiol.* 2014;29:25–32.
56. Kroese JM, Broekhuizen ML, Poelmann RE, Mulder PG, Wladimiroff JW. Epinephrine affects hemodynamics of noninnervated normal and all-trans retinoic acid-treated embryonic chick hearts. *Fetal Diagn Ther.* 2004;19:431–9.
57. Ebert SN, Taylor DG. Catecholamines and development of cardiac pacemaking: an intrinsically intimate relationship. *Cardiovasc Res.* 2006;72:364–74.
58. Kelder TP, Duim SN, Vicente-Steijn R, Vegh AM, Kruithof BP, Smits AM, van Bavel TC, Bax NA, Schalijs MJ, Gittenberger-de Groot AC, et al. The epicardium as modulator of the cardiac autonomic response during early development. *J Mol Cell Cardiol.* 2015;89:251–9.
59. Chen PS, Chen LS, Fishbein MC, Lin SF, Nattel S. Role of the autonomic nervous system in atrial fibrillation: pathophysiology and therapy. *Circ Res.* 2014;114:1500–15.
60. Han S, Joung B, Scanavacca M, Sosa E, Chen PS, Hwang C. Electrophysiological characteristics of the Marshall bundle in humans. *Heart Rhythm.* 2010;7:786–93.
61. Depes D, Mennander A, Vehniäinen R, Paavonen T, Kholová I. Human pulmonary vein myocardial sleeve autonomic neural density and cardiovascular mortality. *J Histochem Cytochem.* 2022;70:627–42.
62. Jongbloed MR, Schalijs MJ, Poelmann RE, Blom NA, Fekkes ML, Wang Z, Fishman GI, Gittenberger-De Groot AC. Embryonic conduction tissue: a spatial correlation with adult arrhythmogenic areas. *J Cardiovasc Electro-physiol.* 2004;15:349–55.
63. Bet BB, De Vries JM, Limpens J, Van Wely M, Van Leeuwen E, Clur SA, Pakrj E. Implications of fetal premature atrial contractions: systematic review. *Ultrasound Obstet Gynecol.* 2022;60:721–30.

## Publisher's Note

Springer Nature remains neutral with regard to jurisdictional claims in published maps and institutional affiliations.